Laser-Induced Breakdown Spectroscopy (LIBS) as a tool for in situ mapping and textural interpretation of lithium in pegmatite minerals

Sweetapple, Marcus T.[1*], Tassios, Steven[2]

[1] *CSIRO, Earth Science and Resource Engineering, PO Box 1130, Perth, Western Australia, 6102*

[2] *CSIRO, Process Science and Engineering, Gate 1, Normanby Rd, Clayton, Victoria, 3169 Australia*

Abstract

Laser-Induced Breakdown Spectroscopy (LIBS) offers an efficient method for qualitative and semi-quantitative analysis of light elements ($Z < 10$), including lithium. This relatively inexpensive analytical tool provides very rapid analysis with little sample damage, requiring minimal sample preparation. In principle, LIBS is a form of atomic emission spectroscopy, relying on characteristic spectra emitted from plasma generated by a high energy laser pulse striking a sample (solid, liquid or gas).

In this study LIBS mapping was applied to petrographically characterised samples of hydrothermally altered spodumene from the Neoarchaean Mt. Cattlin lithium pegmatite deposit. Spodumene ($LiAlSi_2O_6$) is the ore mineral in this deposit, but lithium is distributed in variety of minerals including primary micas and tourmaline, as well as in the alteration mineralogy of

* Present Address: Centre for Exploration Targeting, University of Western Australia, 35 Stirling Highway, Crawley, Perth, W.A., Australia 6009. Email: sweetapple.consulting@gmail.com

spodumene. Mapping was carried out using a grid of analysis spots of 125 μm diameter, spaced at 200 μm intervals, on a sample surface cut by a diamond saw blade without further preparation. Results from mapping of lithium in these samples effectively discriminated between spodumene, its alteration mineralogy, and matrix silicate minerals of the matrix. However, quantification of LIBS results using lithium doped borosilicate glasses as standards was limited due to issues with the sensitivity of matrix matching of standards and self absorption effects at Li_2O values greater than ~2 wt%, especially at values greater than ~6 wt%. The results of this study testify to the effectiveness of LIBS as a mapping tool for light elements, which may be used as a complement to other mapping techniques. Mapping of lithium in pegmatite minerals has important applications in exploration, evaluation and beneficiation of lithium pegmatite ore bodies.

Introduction

Lithium is a problematic element for in situ mineral analysis by most routine microanalytical techniques available to geoscientists. For example, it cannot be detected or analysed as part of routine element suites by energy dispersive spectroscopy (EDS) and electron microprobe analysis (EMPA) since its wavelength lies outside the accessible range for current instrumentation, due to absorption of its low energy characteristic X-ray emission line (e.g. Reed 2005). Other techniques such as Ion or Proton Microprobe, Electron Energy Loss Spectroscopy (EELS), and Secondary Ion Mass Spectrometry (SIMS) and Laser Ablation ICP-MS, which can provide effective lithium analysis, may be difficult to access or impracticable, and may also be expensive. These drawbacks are particularly true in industrial contexts relating to exploration for, and mining and processing of, lithium minerals, where Li content is typically evaluated purely by bulk chemical analyses.

In the case of rare metal granitic pegmatites, particularly the LCT petrogenetic type of Černý (1993) and Černý and Ercit (2005), lithium may be distributed across a number of different mineral species within the same pegmatite, both those having Li as an essential component, such as petalite ($LiAlSi_4O_{10}$), spodumene ($LiAlSi_2O_6$) and amblygonite-montebrasite ($LiAl(PO_4)(F,OH)$), and those minerals having variable amounts of Li substitution, such as di- and trioctahedral micas and tourmaline. The sheer complexity of mineralogical assemblages of granitic pegmatites, combined with the varying stages of primary, secondary, and alteration mineral paragenesis may result in wide ranges of mineralogical and textural variation in lithium distribution in rare metal granitic pegmatites. Such issues become of paramount importance in the interpretation of Li data obtained from whole rock analyses in the aforementioned industrial context. Characterization of distinct Li species is essential when ore beneficiation processes are designed to recover minerals with distinct physical properties such as specific gravity.

The most common approach to obtaining an estimate of lithium content of minerals from microanalytical data is by calculations from quantifiable elements from EMPA data, making use of well-known structural formulae derived from measureable major and minor elements. These calculations typically require normalization, charge balance and/or difference calculations based on other atomic species, or in the case of micas make use of empirical relationships between Li and other elements, such as Mg, F and Si (e.g. Monier and Robert 1986; Tindle and Webb 1990; Tischendorf et al. 1997, 1999). However, all of these calculations are invariably limited by inherent assumptions regarding the extent of site occupancy, presence of site vacancies, substitution relationships, and the oxidation state of iron. A discussion of some different methods

of lithium determinations in minerals may be found in Charoy et al. (1995). In the case of lithium pegmatite minerals, Li concentrations have typically been obtained directly by LA-ICP-MS (e.g. Beurlen et al. 2011, Gadas et al. 2012; Roda Robles et al. 2012), or less commonly, by ion microprobe analyses (e.g. Wilson and Long 1983; Henderson et al. 1989; Charoy et al. 1995).

By extension, spatial (2 or 3D) mapping of lithium distributions in mineral assemblages is similarly problematic. Techniques such as nuclear microprobe, as PIGE (Proton Induced Gamma-ray Emission) (cf. review of Potts et al. 1995), and TOF-SIMS (Time-Of-Flight Secondary Ion Mass Spectrometry) are capable of mapping lithium, but very few studies of light element mapping using these techniques have been carried out with mineralogical applications in mind. Depth homogeneity of lithium and boron in micas and tourmaline, respectively, was studied using nuclear microprobe by Toulhoat et al. (1993). LA-ICP-MS mapping of lithium, over a concentration range of 5-340 ppm, in quartz from precious and base metal ore deposits was carried out by Rusk et al. (2011). TOF-SIMS mapping of low level (< 15 ppm) Li was carried out on serpentinised peridotite by Savov et al. (2006), and by Stephan (2001) on meteorites and their inclusions.

Here we report on a novel application of Laser-Induced Breakdown Spectroscopy (LIBS) as a simple tool for semi-quantitative mapping of lithium mineral distributions in 2D, applied to spodumene and accompanying primary and alteration micas. These minerals have been sampled from the Mt. Cattlin spodumene pegmatite, described by Spiers et al. (2011). Spodumene and its alteration products at Mt. Cattlin were previously studied chemically and crystallographically by Grubb (1963) and Graham (1975). We also report on supporting SEM and EMPA studies that are

used to characterize these lithium bearing minerals. This pegmatite orebody was mined as a source of Li from spodumene between 2010 and 2013. To the best of our knowledge, LIBS has not been used to map specifically Li distributions of minerals in any other published studies to date.

The LIBS technique and its petrological applications

LIBS offers an efficient and powerful method for simultaneous multi-element analysis of materials. Elements that can be detected span the bulk of the periodic table, with excellent coverage of elements with $Z < 13$, including Li, Be and B, which are of interest in the study of rare metal pegmatites. In particular, lithium has strong optical emissivity characteristics which allow effective measurement by the LIBS technique.

In principle, LIBS is a form of atomic emission spectroscopy, relying on characteristic spectra emitted from plasma generated by a high-energy laser pulse striking a sample (solid, liquid or gas). Each pulse produces a high-intensity plasma that is detected by a series of spectrometers, and the resulting emission spectrum contains atomic emission lines from the atomic species present in the plasma. A number of pulses are averaged over a few seconds analysis time to produce an averaged spectrum for the sample being analysed. The spectrometer is able to measure, with varying degrees of sensitivity, almost every element of the periodic table within each laser pulse, subject to the strength of the emission lines. A portion of a typical LIBS spectrum from analysis of spodumene is shown in Figure 1. Quantification is achievable by both conventional calibration methods using defined standards (e.g. chemometric methodology of Death et al. 2009), and also potentially by standardless methods (cf. Harmon et al. 2013 and

115 references therein). The essential components of the LIBS setup and instrumentation are shown
116 diagrammatically in Figure 2.
117
118 Comprehensive overviews of the LIBS technique may be found in Yueh et al. (2000), Myers et
119 al. (2008), Noll (2012), and Musazzi and Perini (2014). Overviews of applications to mineral
120 analysis may be found in McMillan et al. (2007), Harmon et al. (2009, 2013) and Hark and
121 Harmon (2014). In mineralogy, LIBS has found wide application across a range of different
122 mineral types for 'fingerprinting' studies of compositional variants of given species (e.g. Harmon
123 et al. 2006, 2009, 2013; Alvey et al. 2010; Rossi, et al. 2014).
124
125 LIBS has advantages over many other microanalytical tools, for example: little or no sample
126 preparation; accommodation of small sample sizes; detection of trace elements to ppm levels; a
127 modular and readily configurable nature in terms of instrumentation (cf. Harmon et al. 2009;
128 Hark and Harmon 2014). It also produces little damage to samples, consuming nanograms of
129 sample material per laser pulse. Each laser pulse has the potential to detect nearly all elements in
130 a mineral with a suitably configured instrument. LIBS also has the advantage of being able to be
131 readily combined with other analytical techniques such as infra-red and Raman spectroscopies.
132 LIBS instruments are also relatively cheap compared to many other advanced microanalytical
133 tools, with an instrument capable of research grade performance costing between ~US$100,000
134 and US$250,000, with relatively low operating costs. However, these advantages should be
135 contextualized by the disadvantages of LIBS: physical (e.g. density, surface texture, granularity)
136 and chemical (element concentration) matrix effects; the inherent shot-to-shot variability in LIBS
137 experiments; and a level of precision of ~5-20% RSD (Hark and Harmon 2014; Rossi et al.

2014). Precision of LIBS measurements can be affected by issues relating to spectrometer calibration, and plasma effects that can induce broadening in spectral peaks (cf. Noll 2012).

In terms of application to lithian minerals, the seminal study of Fabre et al. (2002) applied LIBS to Li analysis in a variety of geological samples with Li at ppm to % level concentrations, using a lithium spectral line measured at 670.706 nm. These studies included analyses of spodumene, petalite and eucryptite ($LiAlSiO_4$), with Li concentrations measured in the % level; results obtained from most of these lithium specimens were considered to compare well with results from ion microprobe analysis, although relative errors of up to 20% were reported. Pilot studies of Hanson et al. (2008) and Mader and McMillan (2011) have described methodologies and preliminary quantitative analyses of spodumene and lepidolite by LIBS. Investigations of gem quality spodumene, tourmaline and topaz by Rossi et al. (2014) did not find significant conformity with lithium analysis results from LIBS with EMPA and LA-ICP-MS methods, although good agreement was found for Be, B, Al and Si.

Mapping of surfaces by LIBS has found application in a range of scientific disciplines, including biological and materials science studies, especially for metal alloys (e.g. Noll 2012; Musazzi and Perini 2014 and references therein), but application to minerals has been limited. Examples of applications in mineralogical or petrological studies are mapping of the distribution of major and minor elements in granite by Novotny et al. (2008) (Al, Ca, Fe, Mn), and Kim and Lin (2012) (Ba, Pb, Sr, Fe). The former study found a good spatial correlation between elemental patterns of LIBS and LA-ICP-MS data. Menut et al. (2003) mapped Fe, Si and O in volcanic ash, and Ca, Fe and Al were mapped by Rodolfa et al. (2004) in a rhyolite sample, with a view to use in

161 planetary exploration. Quantitative mapping of basnäsite was carried out by Quarles et al. (2014)
162 (F), and by Chirinos et al. (2014) (Si, Ca, Al) in a comparative and complementary 2D and 3D
163 multi-element study with LA-ICP-MS.
164
165 **Sampling and petrological background**
166 Contrasting units of the Neoarchaean Mt. Cattlin rare metal pegmatite group (Western Australia),
167 were sampled at a location approximately 2 km north of the township of Ravensthorpe (Fig. 3).
168 Samples were taken from a primary spodumene unit, and a lepidolite 'replacement' unit, as
169 described by Sofoulis (1958) and Jacobson et al. (2007).
170
171 Spodumene ($LiAlSi_2O_6$), the targeted ore mineral at Mt. Cattlin, mostly occurs as very coarse to
172 megacrystic grains (typically > 50 mm grain size) that formed during early magmatic
173 crystallization of the pegmatite. Although spodumene is the dominant lithium mineral, Li is
174 typically distributed within this pegmatite in a variety of other minerals of varying abundance
175 and significance. These include di- and trioctahedral micas (e.g. muscovite and members of the
176 lepidolite series), members of the tourmaline supergroup, Li-bearing phosphates (amblygonite-
177 montebrasite) and cookeite (lithian chlorite) (Grubb 1963; Jacobson et al. 2007; Spiers et al.
178 2011). Additionally, spodumene alters readily under hydrothermal conditions to produce a range
179 of alteration minerals, typically involving a loss of most Li^+ into solution (Graham 1975; London
180 and Burt 1982a,b; Wood and Williams-Jones 1993), relating to the interaction of spodumene
181 with paragenetically late stage residual pegmatitic fluids containing H^+ and K^+ ions (e.g. London
182 and Burt 1982a; Wood and Williams-Jones 1993; Charoy et al. 2001; Rao et al. 2012).
183 Spodumene is typically replaced to varying extents by 'sericite'/muscovite, quartz, eucryptite

184 ($LiAlSiO_4$), 'adularia', albite and chlorite. Textural changes transitioning between spodumene
185 and its alteration products are graphically described by London and Burt (1982a; their Figure 2).
186 This replacement accompanies color changes in spodumene, typically from white-grey to shades
187 of green and ultimately black, accompanying the destruction of the crystal fabric of spodumene,
188 i.e. the 'rotten spodumene' described by Graham (1975) at Mt. Cattlin. This latter work at Mt.
189 Cattlin showed that spodumene makes a transition to muscovite in three intergrowth orientations
190 controlled by the original spodumene structure. However, in most cases observed, the extent of
191 replacement by this hydrothermal alteration is variable, and often results in a very fine mixture of
192 spodumene fragments and alteration minerals.
193
194 For the purposes of this paper, 'sericite' is used as an informal petrographic term for very fine
195 grained white mica, typically occurring as an alteration or replacement species of primary
196 silicates, usually of muscovite or phengite series compositions but possibly including other
197 mineral species, equivalent to the definition of Eberl et al. (1987). 'Adularia' is used as an
198 informal term to denote low-temperature potassium feldspar alteration that has not been
199 crystallographically defined, but has been characterized by EDS analyses and petrography (cf.
200 Thompson and Thompson 1996). Lepidolite is used as a generalized term for trioctahedral
201 lithium micas of the lepidolite series approximating the composition of trilithonite-polylithonite
202 as per the definition of Rieder et al. (1998).
203
204 ## Analytical Methods
205 ### LIBS

Instrumentation and calibration A Spectrolaser 4000 LIBS system (Laser Analysis Technologies Pty. Ltd.) was used to carry out the lithium mapping and analyses for this study. The LIBS instrument is housed at CSIRO laboratories, Clayton, Victoria. This instrument employs a high power (300 mJ) 1064 nm Nd:YAG Q-switched laser configured for a 532 nm output. The system is equipped with a 4-channel Czerny Turner spectrometer capable of acquiring between 190 nm – 950 nm at a resolution of 0.09 nm at 300 nm. The system has a high precision x-y stepper motor. The lithium peak used for calibration was at a wavelength of 812.644 nm (Fig. 1). This line was selected on the basis of best linear calibration response and lack of interference from other peaks. All analyses were carried out in ambient indoor atmospheric conditions using a laser power of 120 mJ per pulse. Data processing was carried out on software native to the Spectrolaser instrument.

Two different suites of samples were used to construct calibrations that were considered to present reasonable matrix matches to the lithium-bearing silicate minerals analysed. The first suite consisted of a series of synthetic glass standards prepared from a sodium tetraborate flux with various quantities of Li_2O, Al_2O_3, SiO_2, Rb_2O and Cs_2O added. The mixture was fused at 1100°C in a platinum dish and then quenched. The methodology used was identical to that routinely used to make fused beads for XRF analysis.

A second suite comprised of six lithium rock and mineral standards was also used to generate an alternate calibration curve. These standards were pressed as pellets in a 25 mm die to 30 tonnes pressure, and consisted of: certified reference materials (CRMs) NCS86303 and NCS86304 from the China National Analysis Centre for Iron and Steel (2008), certified ISO9001; the OPEG

pegmatite reference material #433 from Geolabs Geoscience Laboratories, Sudbury, Ontario; two split fractions from bulk mica bulk testwork sample T751, and a split fraction from bulk β-spodumene, provided by Galaxy Resources Ltd, and characterized by supplied ICP-MS or -OES analyses. These samples provided a range of 0.058-5.45 wt% Li_2O. All standard samples were split under 'clean lab' conditions.

The two different calibration standards were compared in order to deal with the previously mentioned physical and chemical matrix effects (cf. Hark and Harmon 2014). In LIBS analysis, it is important that not only appropriate chemical matches be made, but also that there is a close morphological match between the calibration standards and the unknown samples. Therefore, differences in density, granularity and surface texture can affect the accuracy of the results, i.e. physical matrix effects. The fused synthetic glass discs more closely match the density of the unknown ore sections, but not the elemental distribution of components such as SiO_2 and Al_2O_3. Conversely, the pressed powders more closely match the chemical compositions, but less so the physical nature of the pegmatite samples.

The results of the two univariate calibrations, both using the Li I 812.644 nm spectral emission line, are shown in Figure 4(a) and (b), for the synthetic glass disc and pressed powder calibrations, respectively. The glass and pressed powder standards achieved an r^2 of 0.994 and 0.999, respectively. It can be seen in the glass calibration (Fig. 4a) that there is a large degree of self-absorption for lithium at high concentrations. This occurs due to the absorption of emission from lithium in the hotter part of the plasma by lithium in the cooler part of the plasma. As a

result, the concentration response is not linear and there is a noticeable plateau at high lithium concentrations.

These two calibrations were then compared with each other by analysing the standard sets of each type with both calibrations, in order to evaluate how well each calibration predicted the composition of the reference standard (Fig. 5a and b). The glass calibration predicts both the glass and pressed powder Li_2O concentrations very well with a close linear fit (R^2 of 0.9165) at levels below approximately 2 wt% (Fig. 5a). There is a notable over-estimation that occurs at higher concentrations due to non-linearity in the calibration caused by lithium self-absorption. The results for the validation of the pressed powder standards were not as good, with a notable underestimation of the Li_2O concentrations of the fused glass disc samples (Fig. 5b).

Averaged analyses for the calibration of the glass discs standards returned relative standard deviations of 3.13 to 11.54 for standards containing 0.02-1.68 wt% Li_2O, and 5.61 to 11.27 for standards containing 3.02-6.85 wt% Li_2O. Relative standard deviations do not show linear increases across these ranges.

The lower practical limit of detection (DL) of lithium (as Li_2O) is calculated to be 240 ppm. This value has been calculated as:

$$DL = 3\sigma/slope$$

where σ is the standard deviation of the intensity of the blank spectra, i.e. where the measureable concentration of the element is zero; slope refers to the gradient of the calibration line, or the slope at concentration zero in the case of calibration curves.

274

275 **LIBS mapping** LIBS mapping studies were carried out on portions of flat rock slabs or
276 billets left over from the preparation of polished thin sections used for petrographic, SEM and
277 EMPA studies. LIBS analyses were carried out on the slab faces opposite to that which EMPA
278 and SEM work was carried out on, so the LIBS analyses would be directly relevant to other data
279 gathered, yet not be potentially affected by the impact of other analytical techniques. The slab
280 faces analysed were not subject to any polishing or further treatment other than the original
281 diamond saw cutting of the blocks. A circular area of approximately 30 mm diameter was
282 available for analysis from each slab, exposed within the sample holder, held in position by
283 clamps.

284

285 The LIBS mapping exercise was carried out initially on sample SMCP112, representative of a
286 portion of a spodumene crystal with a gradational alteration rim of very fine mica, and a quartz
287 matrix. The analysis area was selected to encompass a range of different lithium concentrations
288 accompanying a change in mineralogy, delineated from previous SEM and petrographic studies.

289

290 A grid was constructed over a selected area of 5 x 5 mm, with a raster pattern programmed into
291 the PC driving the LIBS analysis over this area. The outline of the chosen grid was marked on
292 the sample with a pencil outline. Initially, LIBS analysis points at 200 μm spacing were traversed
293 down either side of the area to be mapped, and then photographed under a binocular microscope.
294 Subsequently, the full analysis point set was run, and the grid area was photographed again in
295 order to accurately locate the sample points and to provide mineralogical context to the
296 individual LIBS analysis points. In this way, it was possible to reference each analysis spot to a

297 corresponding grid reference on the sample. The grid was reconstructed with vector drawing
298 software and placed over the sample image with the LIBS analysis points, so individual analysis
299 points could be identified from a sketch of the raster scan path.
300
301 A grid spacing of 200 μm between the centre of each point was used over the 5 x 5 mm area
302 mapped, to provide comprehensive coverage, for a total of 676 analysis spots. The LIBS analysis
303 spot size on silicate minerals averaged ~125 μm (Fig. 6), thus a spacing of ~50 μm was left
304 between each analysis spot (Fig. 7). Depths are estimated indirectly from these SEM images to
305 range from ~10 to 25 μm, dependant on the mineral type encountered. Each analysis point was
306 subject to one burn off laser shot (120 mJ), followed by three analysis shots each comprised of
307 120 mJ energy with a 2 μs delay, which were then averaged into a single spectrum. Each
308 spectrum was stored on the attached PC (cf. Fig. 2) along with its location. The LIBS analysis
309 time for these positions was 2 hours and 38 minutes.
310
311 A further sample (SMCP172) was mapped with LIBS, where petrological information and
312 mineral chemistry was available for the sample and host unit in general, but not for the specific
313 sample face analysed by LIBS. The selected area covered an area of a medium grained lepidolite
314 crystal adjoining part a very coarse altered spodumene grain, and coarse grained 'cleavelandite'
315 albite. In this sample, an area of 4 x 5 mm was chosen over the area of interest, for a total of 546
316 points. All other settings used were identical to those described above. The LIBS analysis time
317 for this map was 2 hours and 7 minutes.
318

The numerical results from both mapping exercises were subsequently compiled in a Microsoft Excel® spreadsheet, and then scaled using the conditional formatting function built into Excel® to generate color maps.

SEM

SEM imaging was conducted using a Phillips XL40 scanning electron microscope with energy dispersive analytical X-ray detection (EDAX) and low-vacuum capabilities, housed at CSIRO ARRC laboratories, W.A. Operating conditions were 30 keV, 0.5 mBar chamber pressure and a working distance of 9-11 mm. The SEM was used in Robinson backscatter imaging mode. EDAX was used to identify the elemental composition of areas of interest on the backscattered image.

EMPA

The chemical composition of spodumene and micas was analysed using a JEOL 8530F field emission electron probe micro-analyser (EPMA) at the Centre for Microscopy, Characterization and Analysis (CMCA), University of Western Australia. Operating conditions used were a 20 kV accelerating voltage and 15 nA beam current. Software Probe for EPMA from Probe Software Inc. was used for setting up and analysing the data. Matrix corrections were based on the phi-rho-zeta calculation of Pouchou and Pichoir (1985). Calibration standards and X-ray lines used were: rutile Ti*K*α, periclase Mg*K*α, wollastonite Si*K*α and Ca*K*α, apatite P*K*α, pollucite Cs*L*α, synthetic rubidium zinc silicate glass (University of Manitoba) Zn*K*α and Rb*L*α, corundum Al*K*α, orthoclase K*K*α, altaite (PbTe) Pb*K*α, synthetic $Gd_3Ga_5O_{12}$ Ga*K*α, celestite

341 Sr*L*α, jadeite Na*K*α, manganese Mn*K*α, iron Fe*K*α, barite Ba*L*α, fluorite F*K*α, thallium iodide,
342 Tl*L*α, and chalcopyrite, Cu*K*α.
343
344 A second data set of mica ('sericite') analyses (samples SMCP03, 12, 23) were carried out using
345 the JEOL JXA-8500F-CL HyperProbe Field Emission Gun instrument at CSIRO analytical
346 laboratories at Clayton, Victoria. Mica analyses used an accelerating voltage of 15 kV and a
347 beam current of 18 nA, with a defocused analysis spot (typically > 50 μm across) to reduce
348 migration of loosely bound ions away from the electron beam. Matrix correction calculations
349 were performed using an XPP implementation of PRZ (phi-rho-zeta of Pouchou and Pichoir
350 1985) used in the data reduction program STRATA. Calibration standards and X-ray lines used
351 were: rutile Ti*K*α, Magalox Al*K*α, Mg*K*α, wollastonite Si*K*α and Ca*K*α, CsI Cs*L*α, synthetic
352 rubidium zinc silicate glass (University of Manitoba) Rb*L*α, adularia K*K*α, apatite P*K*α, NaCl
353 Na*K*α and ClKα, $MnSiO_3$ Mn*K*α, Fe_2O_3 Fe*K*α, barite Ba*L*α, and fluorite F*K*α. Detection limits
354 for elements from both microprobes ranged from 0.01-0.05 wt%; further information is available
355 on request.
356
357 Lithium contents of minerals were estimated by indirect methods using EMPA data, in order to
358 provide constraints on the reasonableness of LIBS results. Methods for indirect estimation of
359 lithium contents for micas use empirically established relationships between lithium and silicon
360 content for trioctahedral micas (Tindle and Webb 1990), or fluorine for dioctahedral micas
361 (Tischendorf et al. 1997) (summarized in Table 1). The relationship of Tindle and Webb (1990)
362 was used in preference to similar empirically established relationships established between
363 lithium and magnesium for trioctahedral micas by Tischendorf et al. (1999), due to the low MgO

364 contents of the micas analysed here, as well as the former relationship returning superior
365 structural formulae. In mica structural formulae, all Fe is assumed to be divalent.
366
367 Calculations of Li content of spodumene has been carried by stoichiometric calculation based on
368 two atoms per formula unit of silicon, with all iron assumed to be in the trivalent state. In the
369 case of SMCP1172 average weight percent totals of spodumene have mean values of 101.4 and
370 101.8 (Table 2). Although this value is within acceptable error limits, it may indicate slightly
371 lower Li contents than have been estimated (assuming accurate determination of Si).
372 Assumptions of all iron being in the trivalent state may also have served to increase the mean
373 total in the case of the more iron rich spodumene from SMCP112. Microprobe results presented
374 here for both spodumene and micas are based on analyses with structural formula recalculations
375 with an error factor of ± 2%. For the purposes of these calculations, analytical results below
376 detection limit are treated as 'zero' for statistical purposes.
377
378 **Results**
379 The maps of lithium distribution (as wt% Li_2O) of the selected areas generated by LIBS analyses
380 are presented in Figures 8 (SMCP112) and 9 (SMCP172), accompanied by photomicrographs of
381 the mapped areas. The analyses constituting these images are calibrated against the glass
382 standards only. Each pixel represents one analysis spot (cf. Fig. 7), which may potentially sample
383 more than one mineral species, both laterally and with respect to depth. Both LIBS maps have
384 been scaled in order to highlight changes in lithium contents with changes in mineralogy.
385

Clearly, the LIBS maps distinguish the variations in lithium content coincident with changes in mineralogy and texture. In Figure 8 (SMCP112), the relationship between mineralogy and lithium distribution is very distinct, and corresponds well to anticipated differences in mineralogy, from spodumene with high lithium grades, to a 'rind' of 'sericite' ± chlorite ± 'adularia' alteration, with greatly reduced lithium content (~0.1-1 wt% Li_2O), and quartz with effectively zero lithium content.

Similarly the LIBS map of SMCP172 (Fig. 9) clearly shows distinctive patterns of lithium distribution, that display relationships to mineralogy in the accompanying photomicrograph. In comparison with the LIBS map of SMCP112, Figure 9 indicates that lithium concentrations are at relatively higher background levels, with all minerals either containing lithium (as Li_2O) at levels > 0.22 wt%, or hosting lithium-bearing inclusions. However, peak values are still in the same order of magnitude of several wt%.

LIBS mapping of lithium using the powder standards was carried out for sample SMCP112 over the same selected area (map not shown). This mapping was less accurate and precise, but still returned the same broad distribution of higher and lower lithium values, with a 'zero region' for quartz. These results are expected, given the cross correlation obtained from analyses of each standard set with each other (cf. Fig. 5), as described in the methods section. Most Li_2O results were in the range ~0-5 wt%, similar to those obtained by the glass standard data (cf. Fig. 8). These results, even with greater physical matrix effects as previously discussed, support the validity of LIBS as a tool of semi-quantitative element mapping. However, there are a number of anomalously high values (~6-11 wt% Li_2O) at the border between mica alteration and quartz, for

409 which no mineralogical explanation can be advanced; additionally Li_2O values > 8 wt% are
410 implausible based on the known mineralogy.
411
412 Results of EMP analyses expressed as data ranges for spodumene, dioctahedral 'sericite' and
413 lepidolite are presented in Tables 2-5. The results of these analyses are utilized to support
414 interpretations of the LIBS maps.
415
416 **Discussion and interpretation of maps**
417 In order to evaluate the performance of the LIBS maps for lithium, it is instructive to compare
418 the lithium contents of the various minerals mapped with data derived from EMP analyses.
419
420 **SMCP112** In the case of SMCP112, the values for the region of spodumene in Figure 8
421 range from ~2-4.2 wt%, with the mapped region taking on a patchy or mottled appearance within
422 the restrictions of the pixelated image. These values are significantly less than the values
423 indicated by recalculation from microprobe data of ~7.7-8.1 wt% Li_2O (Table 2), with the
424 maximum LIBS Li_2O value mapped being 4.2 wt%. This apparent discrepancy may be partially
425 explained by the nature of incipient alteration affecting the spodumene, which may be made out
426 to some degree in the accompanying photomicrograph (Fig. 8). Lighter shades, indicative of
427 unaltered spodumene, broadly correspond to higher Li_2O concentrations, whereas the darker
428 greyish green shades, indicative of 'sericite' dominated alteration, correspond to lower
429 concentrations. Thus these different color shades relate to the extent of microcrystalline internal
430 alteration within the larger spodumene crystal.
431

The texture, grainsize and distribution of this alteration of primary spodumene is illustrated in Figure 10, where very fine grained to cryptocrystalline 'sericite', with minor 'adularia', chlorite and albite, replaces spodumene along cleavage planes, as well as in fractures cross cutting these planes. This photomicrograph is representative of the least altered spodumene seen in the lower right corner of the map in Figure 8. Locally, and towards the margins, this 'sericite' dominated alteration becomes pervasive, ultimately completely replacing spodumene (cf. Fig. 11). The relative intensity of this alteration would suggest that the majority of analysis points in the map grid will contain at least a minor component of this alteration, given the size and coverage of the analysis points (Figs. 6, 7) and the distribution of alteration (Fig. 10).

EMP analyses of 'sericite' from SMCP112 are listed in Table 3, with ranges of values derived from indirect calculations from known structural formulae; Li_2O content averages 0.03 wt% and has a maxima of 0.07 wt% (cf. muscovite analysis of 0.02 wt% Li_2O by wet chemistry, of Graham (1975)). The other subordinate silicate alteration minerals (chlorite, albite, 'adularia') do not contain lithium contents detectable by EMPA, and can be considered to have zero lithium content for practical purposes. No cookeite (lithian chlorite, $LiAl_5Si_3O_{10}(OH)_8$) was detected within spodumene alteration here, although this is known as an alteration mineral of spodumene in pegmatites elsewhere (e.g. Bobos et al. 2007). Thus dilution of spodumene by alteration mineralogy is highly plausible as a mechanism to explain the mapped distribution pattern of Li_2O. However, the pattern of fragmentation of spodumene (Fig. 10) suggests that at least a few of the analysed spots in the area of palest (corresponding to least altered) spodumene should have values close to those determined from the EMP analyses (i.e. ~6-7 wt%). Therefore it is most probable that the peak mapped Li_2O values for spodumene also relate to the previously

455 discussed self-absorption effects of the lithium glass standard calibration curve, at values > ~2
456 wt%, and especially for values > ~6 wt%.
457
458 The outer 'sericite' dominated alteration rim is effectively composed of a pseudomorph of
459 'sericitic' micas after spodumene, often retaining the original crystal shape. Petrographic
460 investigation indicates the retention of original texture from spodumene, including cleavage, as
461 well as the system of irregular alteration fractures (Fig. 11; cf. Fig. 10). These rims and fractures
462 typically also include a minor component of other alteration minerals beside 'sericite', as
463 previously described (Fig. 11), and may also contain traces (typically < 1%) of spodumene
464 fragments. The Li_2O content of most of the 'sericite' dominated rim determined by LIBS
465 analyses is in the order ~0.15 wt% (Fig. 8), which are in the same order of magnitude as the
466 values obtained indirectly from EMPA analyses (0.01-0.07 wt%; Table 3). The higher values
467 from LIBS analyses compared with data derived from EMPA data may be accounted for by
468 greater errors induced by the indirect nature of the EMPA Li_2O calculations and/or cryptic traces
469 of residual spodumene. It is most improbable that such a difference can be accounted for by
470 analytical variations in the LIBS analytical results, given the low standard deviations (0.003-
471 0.011) given by analysis of the calibration standards over these Li_2O concentrations (cf.
472 Instrumentation and Calibration section). Notably, comparable Li_2O values of up to 0.14 wt%,
473 averaging 0.06 wt%, have been derived from EMPA results from analyses of 'sericite' derived
474 from alteration of spodumene from samples elsewhere in the Mt. Cattlin pegmatites (Table 4).
475 Furthermore, data from other alteration muscovite/'sericite' after spodumene from pegmatite
476 occurrences elsewhere have similarly low Li_2O contents (e.g. ≤ 0.05 wt%, Nanping pegmatite,

China, Rao et al. 2012), similar to other late stage pegmatitic white micas (e.g. summary of Hawthorne and Černý 1982).

LIBS analyses of quartz did not indicate any lithium content above the detection limit, consistent with expectations. Values of Li_2O between ~0.04-0.1 wt% along the upper margin of the 'sericite' dominated alteration rim (Fig. 8) are indicative of mixture of 'sericite' and quartz in LIBS analysis spots, and gradational dispersion of 'sericite' into the matrix.

SMCP172 The LIBS map of this sample (Fig. 9) shows some predictable correspondence with mineralogy in the accompanying photomicrograph, but also some unexpected findings with respect to Li_2O distribution. Interpretation of the Li_2O distribution and mineralogy of the sample has been undertaken with data from other samples and EMPA analysis of spodumene and purple alteration mica from material comprising a different part of the same hand sample (Tables 2, 3).

Most prominently, there is a close correspondence between a wedge-shaped silvery grey lepidolite crystal aggregate on the left side of the map (outlined by a dashed line in Fig. 9) and elevated Li_2O values in the ~1.9-5 wt% range, with most values in the ~2.5-3 wt% range. Comparison with the range of Li_2O values estimated from EMPA analysis (Table 5) of 3.78-6.84 wt% (mean 5.28 wt%) suggests that many of these values may be underestimating the Li_2O content. The most likely cause of this relates to truncation of higher Li_2O values by self-absorption effects within the calibration, as previously discussed for spodumene from SMCP112. Petrographic observations of lepidolite in other samples do not suggest significant alteration, as

499 in the case of spodumene, although a component of intergrowth with other non-lithium bearing
500 silicate minerals is a possible contributor.
501
502 Very fine grained purple micas as an alteration product of spodumene occupy the bulk of the left
503 hand side of the map (Fig. 9), wrapping around the wedge-shaped lepidolite aggregate. LIBS
504 analyses of this altered spodumene broadly return relatively uniform values in the 0.9-1.6 wt%
505 Li_2O range. Petrography suggests that this alteration is relatively uniform and pervasive, and
506 texturally analogous to that seen in Figure 11 for SMCP112. Calculation Li_2O contents from
507 microprobe analyses of this mica in another fragment of the sample with the same alteration
508 (Table 3) yield very low Li_2O contents, ranging from less than detection to 0.02 wt%, with a
509 mean value of ~0.01 wt%. Although some EMPA results have relatively low weight percent
510 totals (a number returning totals of 97-98 wt%), and slightly depleted octahedral sites (Y=3.94-
511 4.0), it is not possible to comment further on the relative accuracy of the Li_2O calculations given
512 that these results lie with the envelope of error. These results are also within the same order of
513 magnitude as dioctahedral micas replacing spodumene from other samples (Tables 3 and 4).
514 However, the LIBS values are considered not implausible, given the common occurrence of relic
515 spodumene fragments in other samples (cf. SCMP112; Fig. 11), which may be dispersed
516 amongst masses of alteration micas. The central pink mica grain, contiguous with the previously
517 discussed lepidolite aggregate, tentatively identified visually as a rose muscovite, had relatively
518 low Li_2O values of ~0.7-1.6 wt%. Although we do not have comparative data derived from
519 EMPA for this pink mica, these values are within the ranges of known rose or lithian pegmatitic
520 muscovites elsewhere (e.g. Hawthorne and Černý 1982).
521

522 It is important to state the purple or pink coloration of micas does not relate to their lithium
523 contents as popularly believed, but is related to the interplay between the dominance of Mn over
524 Fe, and the oxidation states of Fe and other transition metal chromophores (Finch et al. 1982;
525 Hawthorne and Černý 1982; Jolliff et al. 1987; Fleet 2003).
526
527 LIBS mapping of lithium across the variably altered, mottled green spodumene grain occupying
528 much of the right side of the mapped area (Fig. 9) reveals changes in lithium distribution which
529 in most cases corresponds to changes in color within the spodumene crystal in hand specimen, as
530 per spodumene in SMCP112. Again, lighter green corresponds to higher Li_2O concentrations,
531 whereas the darker green shades correspond to lower concentrations. However, LIBS mapping
532 shows up subtle changes in Li_2O, and therefore mineralogy, not evident in the photomicrograph.
533 However, it is probable that these color changes may also reflect content of other subordinate
534 alteration minerals such as chlorite. Estimations of Li_2O concentrations from LIBS spots of the
535 'sericite' dominated alteration of this grain range from ~0.5-1.6 wt%; most of these values are
536 much greater than analyses of typical spodumene alteration 'sericite' (Tables 3, 4), and the
537 comparable alteration rim of SMCP112 (Fig. 8). Thus it is inferred that these higher values relate
538 to alteration micas with greater Li_2O content and/or inclusions of relic spodumene. The LIBS
539 map (Fig. 9) shows a few distinct spots of ~2.8-3.6 wt% Li_2O within the mottled green
540 spodumene crystal, corresponding to the least altered (paler) regions. Given that higher Li_2O
541 values were returned within lepidolite (~4-5 wt%), it is most probable that these LIBS Li_2O
542 values are reasonable for this altered spodumene, as they lie below the level (of ~6 wt%) where
543 self-absorption has the strongest effects on the calibration curve. Certainly Li_2O values of pure
544 spodumene fragments calculated from EMPA analyses (Table 2) from another location within

545 the same sample (SMCP172) return very similar values to those of SMCP112, as clear indicators
546 of expected Li_2O contents.
547
548 Perhaps the most unexpected result from the lithium mapping exercise of SMCP172 is the
549 indication of elevated level Li_2O contents ($\geq$ 0.22 wt%) over the area of 'cleavelandite' albite on
550 the bottom left edge of the map. LIBS mapping clearly outlines the distribution of the white
551 'cleavelandite' in the photomicrograph in comparison with the LIBS map. This distribution is
552 particularly emphasized due to adjustment of the color scaling of the map, highlighting
553 differences in lithium concentration (Fig. 9). These lithium results for 'cleavelandite' are
554 inconsistent with its known mineral chemistry of albite (e.g. average and maximum documented
555 contents of 13 and 200 ppm Li_2O respectively, database of Smith and Higgins 2010) and the
556 limited degree of crystal chemical compatibility of lithium in the plagioclase crystal lattice (cf.
557 Shannon 1976). Therefore, the most likely explanation is the presence of micro-inclusions of
558 lithium-bearing micas within the 'cleavelandite', either as primary inclusions along twin planes
559 or as microcrystalline disseminations related to alteration (e.g. of adjoining spodumene).
560
561 In summary, LIBS mapping of this sample has returned plausible results that can be explained
562 from mineral analyses and known petrological features, but with some higher Li_2O values
563 truncated by self-absorption effects inherent in the calibration. The wide distribution of lithium
564 values indicated by mapping is considered to be reasonable based on known lithium enrichment
565 in lepidolite-rich units in the Mt. Cattlin pegmatite.
566
567 **Conclusions**

We demonstrate in this article that LIBS is a powerful tool for semi-quantitative mapping of lithium oxide concentrations in silicate minerals. These maps, comprised of closely spaced analysis points, were carried out with a minimal amount of sample preparation, and are virtually non-destructive. The size of LIBS maps is limited only by computing power and the physical limitations of the sample holder.

The LIBS maps demonstrated here effectively discriminated between spodumene, its accompanying 'sericite' alteration, lepidolite and matrix minerals (quartz and albite), in samples of lithium-rich granitic pegmatites. These maps were able to be meaningfully related to photomicrographs and textural observations of samples characterized by petrology. Results obtained from LIBS analyses in the range of ~0.01-5 wt% from analysis of these mineral suites gave reasonable results based on a calibration curve using lithium doped borosilicate glasses, with reference to constraints provided by electron microprobe analysis, and external datasets. However, quantification of LIBS results using lithium doped borosilicate glasses as standards was restricted at Li_2O values > ~2 wt%, and especially at values > ~6 wt%, primarily due to self absorption effects, and secondly, matrix matching of standards. These results validate the basic capability of the LIBS method as a semi-quantitative analytical tool for mapping, although further refinement is required with respect to calibration for full quantification.

Implications

This study demonstrates the effectiveness of LIBS as a mapping tool for light elements, which may be used to complement other mineral mapping techniques, such as EDS X-ray mapping of rocks and minerals in situ. The minimal amount of sample preparation and flexibility of the LIBS

591 technique potentially allow it to be taken into other geologic and industrial environments where
592 Li and other light elements are encountered, e.g. assessment of brine deposits.
593
594 LIBS mapping of light elements including lithium, has considerable application in an industrial
595 context, where LIBS can potentially provide very rapid information that can inform time critical
596 processes in mining and ore beneficiation. Examples of this include grade control during mining
597 and assessment of concentrate grades after crushing and screening of fractions of spodumene and
598 other light element bearing minerals. Naturally, results of spatially referenced LIBS analysis
599 points can be referred back to visual observations of minerals made by geologists during
600 exploration and mining, to improve workflows.
601

602 **Acknowledgements**

603 The authors thank Nancy McMillan and Alexandre Lima for their insightful reviews of this
604 paper. Joanna Parr and Yulia Uvarova (CSIRO Earth Science and Engineering) are thanked for
605 their reviews of an earlier version of this article. Fernando Colombo is thanked for his editorial
606 oversight and additional detailed review. We acknowledge the support of Galaxy Resources Ltd.
607 for this study, which was carried out as part of a larger research project. We thank Phil
608 Tornatora, Tim Leonard (Galaxy) and Mike Grigson (Consulting Geologist) for their support of
609 research into the Mt. Cattlin lithium orebody. Doug Body (Independent LIBS consultant) is
610 particularly thanked for expert advice in support of the LIBS analyses, including calibration, and
611 David Death and Pavel Yaroshchyk (CSIRO Process Science and Engineering) are thanked for
612 initial investigations of the LIBS technique. Steve Barnes and Joanna Parr (CSIRO Earth Science
613 and Engineering) are thanked for their encouragement to write this paper. Michael Verrall

(CSIRO Earth Science and Engineering) is thanked for assistance with SEM work. The authors acknowledge the use of the electron microprobe facilities at CSIRO Process Science and Engineering, Clayton, and technical assistance of Colin McRae, and at the Australian Microscopy & Microanalysis Research Facility of the University of Western Australia, with the technical assistance of David Adams. The latter facility at UWA is within the Centre for Microscopy, Characterisation & Analysis, a facility funded by the University, State and Commonwealth Governments. Data handling of microprobe analyses was carried out using modified versions of Microsoft Excel® spreadsheets devised by A.G. Tindle of the Open University, Milton Keynes, U.K (available from http://www.open.ac.uk/earth-research/tindle/AGTWebPages/AGTSoft.html; website accessed April 2014).

References

Alvey, D.C., Morton, K., Harmon, R.S., Gottfried, J.L., Remus, J.J., Collins, L.M., and Wise, M.A. (2010) Laser-induced breakdown spectroscopy-based geochemical fingerprinting for the rapid analysis and discrimination of minerals: the example of garnet. Applied Optics, 49, C168-C180.

Beurlen, H., Muller, A., Silva, D., and Da Silva, M. (2011) Petrogenetic significance of LA-ICP-MS trace-element data on quartz from the Borborema Pegmatite Province, northeast Brazil. Mineralogical Magazine, 75, 2703-2719.

Bobos, I., Vieillard, P., Charoy, B., and Noronha, F. (2007) Alteration of spodumene to cookeite and its pressure and temperature stability conditions in Li-bearing aplite-pegmatites from northern Portugal: Clays and Clay Minerals, 55, 295-310.

636 Černý, P. (1993) Rare-element granitic pegmatites. Part I: Anatomy and internal evolution of
637 pegmatite deposits. In P.A. Sheahan and M.A. Cherry eds., Ore Deposit Models Volume II.
638 Reprint Series 6, Geoscience Canada, 29-47.
639 Černý, P., and Ercit, T.S. (2005) The classification of granitic pegmatites revisited. Canadian
640 Mineralogist, 43, 2005-2026.
641 Charoy, B., Chaussidon, M., and Noronha, F. (1995) Lithium zonation in white micas from the
642 Argemela microgranite (central Portugal): an in-situ ion-, electron-microprobe and
643 spectroscopic investigation. European Journal of Mineralogy, 7, 335-352.
644 Charoy, B., and Noronha, F. (1996) Multistage growth of a rare-element, volatile-rich
645 microgranite at Argemela (Portugal). Journal of Petrology, 37, 73-94.
646 Charoy, B., Noronha, F., and Lima, A. (2001) Spodumene-petalite-eucryptite: mutual
647 relationships and pattern of alteration in Li-rich aplite-pegmatite dykes from northern
648 Portugal. Canadian Mineralogist, 39, 729-746.
649 Chirinos, J.R., Oropeza, D.D., Gonzalez, J.J., Hou, H., Morey, M., Zorba, V., and Russo, R.E.
650 (2014) Simultaneous 3-dimensional elemental imaging with LIBS and LA-ICP-MS.
651 Journal of Analytical Atomic Spectrometry, 29, 1292-1298.
652 Death, D., Cunningham, A., and Pollard, L. (2009) Multi-element and mineralogical analysis of
653 mineral ores using laser induced breakdown spectroscopy and chemometric analysis.
654 Spectrochimica Acta Part B: Atomic Spectroscopy, 64, 1048-1058.
655 Eberl, D.D., Srodon, J., Lee, M., Nadeau, P.H., and Northrop, H.R. (1987) Sericite from the
656 Silverton Caldera, Colorado: Correlation among structure, composition, origin, and particle
657 thickness. American Mineralogist, 72, 914-934.

Fabre, C., Boiron, M.-C., Dubessy, J., Chabiron, A., Charoy, B., and Martin Crespo, T. (2002) Advances in lithium analysis in solids by means of laser-induced breakdown spectroscopy: an exploratory study. Geochimica et Cosmochimica Acta, 66, 1401-1407.

Finch, J., Gainsford, A.R., and Tennant, W.C. (1982) Polarized optical absorption and ^{57}Fe Mossbauer study of pegmatitic muscovite. American Mineralogist, 67, 59-68.

Fleet, M.E. (2003) Micas: rock forming minerals, Volume 3A. London, Geological Society of London, 758 p.

Gadas, P., Novak, M., Stanek, J., Filip, J., and Vasinova Galiova, M. (2012) Compositional evolution of zoned tourmaline crystals from pockets in common pegmatites of the Moldanubian Zone, Czech Republic. Canadian Mineralogist, 50, 895-912.

Graham, J. (1975) Some notes on alpha-spodumene, $LiAlSi_2O_6$. American Mineralogist, 60, 919-923.

Grigson, M. (2009) Regional geological map of the Mt. Cattlin area. Unpublished consultant's report to Galaxy Resources Ltd.

Grubb, P.L.C. (1963) Spodumene from Ravensthorpe and Mt. Marion, Western Australia – a mineralogical and chemical Study. CSIRO Mineragraphic Investigations Reports, CSIRO, 16 p.

Hanson, A., McMillan, N.J., and Wise, M.A. (2008) Quantitative analysis of Li by laser induced breakdown spectroscopy. Geological Society of America 2008 annual meeting, 40, p. 176.

Hark, R.R., and Harmon, R.S. (2014) Geochemical fingerprinting using LIBS. In S. Musazzi and P. Perini, Eds., Laser-Induced Breakdown Spectroscopy - Theory and Applications, Spinger Series in Optical Sciences, 182, Berlin Heidelberg, Springer, p. 309-348.

Harmon, R.S., DeLucia, F.C., McManus, C.E., McMillan, N.J., Jenkins, T.F., Walsh, M.E., and Miziolek, A. (2006) Laser-induced breakdown spectroscopy - An emerging chemical sensor technology for real-time field-portable, geochemical, mineralogical, and environmental applications. Applied Geochemistry, 21, 730-747.

Harmon, R.S., Remus, J., McMillan, N.J., McManus, C., Collins, L., Gottfried, J.L. Jr., DeLucia, F.C., and Miziolek, A.W. (2009) LIBS analysis of geomaterials: geochemical fingerprinting for the rapid analysis and discrimination of minerals. Applied Geochemistry, 24, 1125-1141.

Harmon, R. S., Russo, R.E., and Hark, R.R. (2013) Applications of laser-induced breakdown spectroscopy for geochemical and environmental analysis: A comprehensive review. Spectrochimica Acta Part B: Atomic Spectroscopy, 87, 11-26.

Hawthorne, F. C., and Černý, P. (1982) The mica group. In P. Černý, Ed., Granitic Pegmatites in Science And Industry, 8. MAC Short Course Series, Winnipeg, Mineralogical Association of Canada, p. 63-98.

Henderson, C. M., Martin, J.S., and Mason, R.A. (1989) Compositional relations in Li-micas from S.W. England and France: an ion- and electron-microprobe study. Mineralogical Magazine, 53, 427-449.

Jacobson, M.I., Calderwood, M.A., and Grguric, B.A. (2007) A guidebook to the pegmatites of Western Australia. Perth, Hesperian Press, 356 p.

Jolliff, B.L., Papike, J.J., and Shearer, C.K. (1987) Fractionation trends in mica and tourmaline as indicators of pegmatite internal evolution: Bob Ingersoll pegmatite, Black Hills, South Dakota. Geochimica et Cosmochimica Acta, 51, 519-534.

Kim, T., and Lin, C.-T. (2012) Laser-induced breakdown spectroscopy. In M. A. Farrukh, Ed., Advanced Aspects of Spectroscopy, InTech, p. 131-164.

London, D., and Burt, D.M. (1982a) Alteration of spodumene, montebrasite and lithiophilite in pegmatites of the White Pichaco District, Arizona. American Mineralogist, 67, 97-113.

London, D., and Burt, D.M. (1982b) Chemical models for lithium aluminosilicate stabilities in pegmatites and granites. American Mineralogist, 67, 494-509.

Mader, S., and McMillan, N.J. (2011) Lithium analysis: the potential application of laser induced breakdown spectroscopy (LIBS). 2011 Geological Society of America Annual Meeting, Minneapolis, 43, p. 89.

McMillan, N.J., Harmon, R.S., De Lucia, F.C., and Miziolek, A.M. (2007) Laser-induced breakdown spectroscopy analysis of minerals: Carbonates and silicates. Spectrochimica Acta Part B: Atomic Spectroscopy, 62, 1528-1536.

Menut, D., Fichet, P., Lacour, J.-L., Rivoallan, A., and Mauchien, P. (2003) Micro-laser-induced breakdown spectroscopy technique: a powerful method for performing quantitative surface mapping on conductive and nonconductive samples. Applied Optics, 42, 6063-6071.

Monier, G., and Robert, J.-L. (1986) Muscovite solid solutions in the system K_2O-Li_2O-MgO-FeO-Al_2O_3-SiO_2-H_2O-HF at 600 C, 2 kbar PH_2O: comparison with natural lithium micas: Mineralogical Magazine, 50, 641-651.

Musazzi, S., and Perini, P. (2014) LIBS instrumental techniques. In S. Musazzi and P. Perini, Eds., Laser-Induced Breakdown Spectroscopy - Theory and Applications, Springer Series in Optical Sciences, 182, p. 59-89, Berlin Heidelberg, Springer.

Myers, M.J., Myers, J.D., and Myers, A.G. (2008) Laser induced breakdown spectroscopy (LIBS). In M. Lackner, Ed., Lasers in Chemistry, 1, p. 313-325, Wiley-VCH.

Noll, R. (2012) Laser induced breakdown spectroscopy - fundamentals and applications. Berlin Heidelberg, Springer, 543 p.

Novotny, K., Kaiser, J., Galiova, M., Konecna, V., Novotny, J., Malina, R., Liska, M., Kanicky, V., and Otruba, V. (2008) Mapping of different structures on large area of granite sample using laser-ablation based analytical techniques, an exploratory study. Spectrochimica Acta Part B: Atomic Spectroscopy, 63, 1139-1144.

Potts, P.J., Bowles, J.F., Reed, S.J., and Cave, M.R. (1995) Microprobe Techniques in the Earth Sciences. London, Mineralogical Society series, 6, Chapman and Hall, 419 p.

Pouchou, J., and Pichoir, F. (1985) PAP (phi-rho-Z) procedure for improved quantitative microanalysis. In J.T. Armstrong, Ed., Microbeam Analysis - 1985, San Francisco Press, p. 104-106.

Quarles, C.D., Gonzalez, J.J., East, L.J., Yoo, J.H., Morey, M., and Russo, R.E. (2014) Fluorine analysis using Laser Induced Breakdown Spectroscopy (LIBS). Journal of Analytical Atomic Spectrometry, p. 5.

Rao, C., Wang, R.C., Zhang, A.C., and Hu, H. (2012) The corundum + tourmaline nodules related to hydrothermal alteration of spodumene in the Nanping No. 31 pegmatite dyke, Fujian Province, southeastern China. Canadian Mineralogist, 50, 1623-1635.

Reed, S.J.B. (2005) Electron Microprobe Analysis and Scanning Electron Microscopy in Geology. Cambridge University Press, 212 p.

Rieder, M., Cavazzini, G., D'Yakonov, Y.S., Frank-Kamanetskii, V.A., Gottardi, G., Guggenheim, S., Koval, P.V., Muller, G., Neiva, A.M.R., Radoslovich, E.W., Robert, J.L., Sassi, F.P., Takeda, H., Weiss, Z. & Wones, D.R. (1998) Nomenclature of the Micas. Canadian Mineralogist, 36, 41-48.

748 Roda-Robles, E., Pesquera, A., Gil-Crespo, P., and Torres-Ruiz, J. (2012) From granite to highly
749 evolved pegmatite: a case study of the Pinilla de Fermoselle granite pegmatite system
750 (Zamora, Spain). Lithos, 153, 192-207.
751 Rodolfa, C., Cremers, D., and Ebinger, M. (2004) In-situ 1-D and 2-D mapping of soil core and
752 rock samples using the LIBS long spark. Abstract #1777: Lunar and Planetary Science
753 XXXV Conference Abstracts, Houston, Texas.
754 Rossi, M., Dell'Aglio, M., De Giacomo, A., Gaudiuso, R., Senesi, G. S., De Pascale, O.,
755 Capitelli, F., Nestola, F., and Ghiara, M.R. (2014) Multi-methodological investigation of
756 kunzite, hiddenite, alexandrite, elbaite and topaz, based on laser-induced breakdown
757 spectroscopy and conventional analytical techniques for supporting mineralogical
758 characterization. Physics and Chemistry of Minerals, 41, 127-140.
759 Rusk, B., Koenig, A., and Lowers, H. (2011) Visualizing trace element distribution in quartz
760 using cathodoluminescence, electron microprobe, and laser ablation-inductively coupled
761 plasma-mass spectrometry. American Mineralogist, 96, 703-708.
762 Savov, I.P., Rost, D., Vicenzi, E.P., and Zack, T. (2006) Microscale Mapping of Boron and
763 Lithium in the Mariana sub-arc Mantle via ToF-SIMS. American Geophysical Union, Fall
764 Meeting 2007.
765 Shannon, R. D. (1976) Revised effective ionic radii and systematic studies of interatomic
766 distances in halides and chalcogenides. Acta Crystallographica, A32, 751-767.
767 Smith, D. G. W., and Higgins, M. D. (2010) MinIdent for Windows, version 4.0.0.41
768 professional, database 1.6. Edmonton, Alberta, Micronex Mineral Services Ltd.
769 Sofoulis, J. (1958) The geology of the Phillips River Goldfield, W.A. Geological Survey of
770 Western Australia, Bulletin 110, 240 p.

Spiers, R., Peters, J., and Lorenzen, L. (2011) Galaxy Resources Mt. Cattlin (Western Australia) project no. 2541. NI43-101 technical report to Canadian Securities Regulators public data register (SEDAR), 212 p.

Stephan, T. (2001) TOF-SIMS in cosmochemistry. Planetary and Space Science, 49, 859-906.

Thompson, A.J.B., and Thompson, J.F.H. (1996) Atlas of alteration. Geological Association of Canada, 119 p.

Tindle, A.G., and Webb, P.C. (1990) Estimation of lithium contents in trioctahedral micas using microprobe data: application to micas from granitic rocks. European Journal of Mineralogy, 2, 595-610.

Tischendorf, G., Forster, H.-J., and Gottesmann, B. (1999) The correlation between lithium and magnesium in trioctahedral micas: improved equations for Li2O estimation from MgO data. Mineralogical Magazine, 63, 57-74.

Tischendorf, G., Gottesmann, B., Forster, H.-J., and Trumbull, R.B. (1997) On Li-bearing micas: estimating Li from electron microprobe analyses and an improved diagram for graphical representation. Mineralogical Magazine, 61, 809-834.

Toulhoat, N., Courel, P., Trocellier, P., and Gosset, J. (1993) Stability and distribution of lithium and boron in minerals. Nuclear Instruments and Methods in Physics Research Section B: Beam Interactions with Materials and Atoms, 77, 436-443.

Whitney, D. L., and Evans, B.W. (2010) Abbreviations for names of rock-forming minerals: American Mineralogist, 95, 185-187.

Wilson, G., and Long, J. (1983) The distribution of lithium in some Cornish minerals: ion microprobe measurements. Mineralogical Magazine, 47, 191-199.

Witt, W.K. (1997) Geology of the Ravensthorpe and Cocanarup 1:100,000 sheets. 1:100,000 Geological Series Explanatory Notes series, Geological Survey of Western Australia, 26 p.

Witt, W.K. (1998) Geology and Mineral Resources of the Ravensthorpe and Cocanarup 1:100,000 sheets: Report 54, Geological Survey of Western Australia, 154 p.

Wood, S.A., and Williams-Jones, A.E. (1993) Theoretical studies of the alteration of spodumene, petalite eucryptite and pollucite in granitic pegmatites: exchange reactions with alkali feldspars. Contributions to Mineralogy and Petrology, 114, 255-263.

Yueh, F.-Y., Singh, J.P., and Zhang, H. (2000) Laser Induced Breakdown Spectroscopy, Elemental Analysis. In R.A. Meyers, Ed., Encyclopedia of Analytical Chemistry, Chichester, John Wiley and Sons Ltd., p. 2066-2087.

Figure captions

Figure 1. Example of a portion of a LIBS spectrum from analysis of spodumene (sample SMCP112), over the spectral range of 580-850 nm, including the 812.644 nm lithium line used for calibration here. The relative spectral intensity unit on the y-axis is given in arbitrary units (a.u.), as relative units of intensity. Note that peak intensities have no relationship to element concentration, for instance Rb and K would be expected to have negligible concentrations in spodumene, although these could relate to mica inclusions.

Figure 2. Schematic diagram of the essential elements of the LIBS system.

Figure 3. Geological plan of the rock relationships interpreted at surface in the area of the Mt. Cattlin mine (adapted from Grigson 2009; Spiers et al. 2011), with sample locations shown. The bracketed negative figure indicates the depth below surface from which the samples were taken

816 from open pit exposures of pegmatite. Pegmatite sheets dip gently to the southwest. Geological
817 units referred to in the legend are those described by Witt (1997, 1998). The area outlined by the
818 black dashed line indicates Galaxy's final proposed open pit design.
819

820 **Figure 4.** LIBS calibration curves (mean peak area vs. concentration) with lines of fit plotted for
821 lithium (812.644 nm line) for (a) synthetic glass standards ($R^2 = 0.994$); (b) pressed powder
822 standards ($R^2 = 0.999$). Concentration for both graphs is weight percent Li_2O.
823

824 **Figure 5.** Scatter plots of comparative analyses between glass disc and pressed powder
825 standards, for (a) analysis of glass and pressed powder standards using the glass disc calibration;
826 (b) analysis of glass and pressed powder standards using the pressed powder calibration.
827

828 **Figure 6.** Backscattered SEM image of a typical LIBS analysis spot in fine grained albite-
829 'sericite' alteration of spodumene, from LIBS map of sample SMCP112. Note that these LIBS
830 analysis spots are typically visible to the unaided eye, dependant on mineralogy and grainsize.
831

832 **Figure 7.** Backscattered SEM image showing detail of close spaced LIBS points used in
833 mapping of sample SMCP112. Mineralogy is very fine albite-'sericite' (upper part of image) and
834 spodumene (lower right corner), displaying strong cleavage. Note spots in the lower part of the
835 image, where surficial micas/albite has been removed by the LIBS analysis spot, exposing
836 spodumene with visible cleavage beneath.
837

838 **Figure 8.** Photomicrograph (left) and corresponding false colored LIBS map of lithium
839 distribution (right) from the selected area of sample SMCP112. The sample mineralogy is
840 labelled in the photomicrograph (abbreviations of Whitney and Evans 2010) with pale white-
841 green spodumene with incipient alteration at bottom, with a rind of dull khaki 'sericite' alteration
842 (±'adularia' ± chlorite) forming a rind on spodumene, and grey quartz of the host matrix is at the
843 top of the image. Each pixel (200 μm squares) on the map represents a corresponding LIBS spot
844 on the sample image to the left (cf. Fig. 7). The numerical scale is weight percent Li_2O. Note that
845 the color scaling of the map is non-linear in order to highlight the correspondence between
846 mineralogy and Li_2O concentration.
847

848 **Figure 9.** Photomicrograph (left) and corresponding false colored LIBS map of lithium
849 distribution (right) from the selected area of sample SMCP172. The sample mineralogy is
850 labelled in the photomicrograph (abbreviations of Whitney and Evans 2010) with pale green
851 weakly altered spodumene in the lower right, and more strongly altered spodumene in the upper
852 right. Spodumene with replacement by very fine purple mica (lepidolite?) is present on the left
853 half of the photomicrograph, with lepidolite and related micas in the centre, and ('cleavelandite')
854 albite at the bottom. This image highlights the lower Li_2O levels associated with albite, and
855 'sericite'± chlorite alteration of spodumene. The numerical scale is weight percent Li_2O, with a
856 non-linear colour scaling to highlight differences in lithium distribution (cf. Fig. 8).
857

858 **Figure 10.** Cross polarized transmitted light photomicrograph of spodumene from SMCP112,
859 displaying typically weak alteration to 'sericite' along cleavage planes (NW-SE orientation) and

irregular cross cutting fractures, with subordinate alteration to chlorite and 'adularia' (as indicated). A subordinate component of albite is also likely within the alteration assemblage.

Figure 11. Cross polarized transmitted light photomicrograph of strongly altered spodumene from SMCP112, displaying pervasive crystallographically controlled replacement by 'sericite' (cf. Graham 1975); note the preservation of spodumene cleavage in the same orientation as shown in Figure 10, as well as irregular cross-cutting fractures. Chlorite, 'adularia' and albite form minor components of the alteration assemblage (as indicated). The locally strong cleavage in the lower left corner suggests the presence of minor spodumene relicts. Strained quartz in the top right corner is representative of the matrix of the original spodumene crystal.

Tables to accompany Sweetapple & Tassios LIBS lithium mapping paper

Table 1: Methods of lithium estimation for dioctahedral and trioctahedral micas, with attribution.

Source	Calculation	Criteria
Tischendorf et al. (1997)	$Li_2O = 0.3935 \times F^{1.326}$	F = 0.01 to 8 wt% Dioctahedral class
Tindle and Webb (1990)	$Li_2O = (0.287 \times SiO_2) - 9.552$	MgO < 3 wt%* SiO_2 > 34 wt%* Trioctahedral class

*recommended application range by Tischendorf et al. (1999)

Table 2: Compositional data range (minima, maxima, mean and standard deviation) for spodumene from electron microprobe analysis. All Fe is treated as Fe_2O_3 for calculation purposes, and all values are listed as weight percent. Titanium was sought but not detected.

	SMCP112 n=5					SMCP172 n=16			
	MIN	MAX	MEAN	STD DEV		MIN	MAX	MEAN	STD DEV
SiO2	61.30	64.80	62.54	1.34		63.74	66.57	66.04	0.67
Al2O3	27.54	27.76	27.68	0.08		25.82	27.59	27.20	0.42
Fe2O3	1.13	1.30	1.23	0.07		0.05	0.10	0.08	0.04
MnO	0.20	0.29	0.24	0.04		0.00	0.00	0.00	0.00
MgO	0.00	0.00	0.00	0.00		0.19	0.19	0.19	0.00
CaO	0.00	0.00	0.00	0.00		0.13	0.23	0.18	0.07
Na2O	0.14	0.18	0.16	0.01		0.07	0.15	0.12	0.02
K2O	0.00	0.11	0.04	0.06		0.01	0.79	0.20	0.31
Li2O§	7.74	8.11	7.98	0.14		7.19	7.84	7.71	0.16
Total	98.78	101.75	99.85	1.75		99.58	101.73	101.23	1.70

§ calculation by stoichiometry; Li ions calculated on the basis of Li = 1-(Na+K+Ca)

Table 3: Compositional data range (minima, maxima, mean and standard deviation) for dioctahedral micas ('sericite'), as alteration of spodumene, from electron microprobe analysis. All values are listed as weight percent. The data set from SMCP172 is representative of the fine purple micas replacing spodumene.

	SMCP112 n=7					SMCP172 n=4			
wt%	MIN	MAX	AVE	STD DEV	wt%	MIN	MAX	AVE	STD DEV
SiO2	48.64	52.51	51.04	1.24	SiO2	46.93	47.61	47.21	0.33
Al2O3	26.40	28.60	27.09	0.87	Al2O3	33.02	34.97	33.84	0.92
FeO	2.05	3.16	2.64	0.44	FeO	0.12	0.12	0.12	0.00
MnO	0.10	0.31	0.22	0.07	MnO	0.14	0.28	0.20	0.06
MgO	2.14	3.59	2.83	0.57	MgO	0.83	1.22	0.96	0.18
CaO	0.04	0.15	0.11	0.04	CaO	0.03	0.10	0.06	0.03
Na2O	0.06	0.55	0.17	0.18	Na2O	0.07	0.16	0.12	0.04
K2O	10.07	11.29	10.71	0.40	K2O	10.01	10.75	10.27	0.33
BaO	0.00	0.11	0.02	0.04	BaO	0.00	0.04	0.01	0.02
Rb2O	0.28	0.51	0.38	0.08	Rb2O	1.23	1.61	1.38	0.16
Cs2O	0.00	0.04	0.03	0.01	Cs2O	0.04	0.10	0.06	0.03
F	0.06	0.27	0.15	0.08	F	0.00	0.11	0.06	0.05
TlO	0.00	0.00	0.00	0.00	TlO	0.00	0.04	0.01	0.02
Li2O*	0.01	0.07	0.03	0.02	Li2O*	0.00	0.02	0.01	0.01
H2O**	4.23	4.52	4.39	0.09	H2O**	4.36	4.45	4.42	0.04
Total***	98.08	101.14	99.76	1.20	Total***	98.20	99.54	98.64	0.61

*Li_2O calculation by the method of Tischendorf et al. (1997)

**H_2O calculation by the method of Tindle and Webb (1990), based on a back-calculation from OH estimated by assuming full site occupancy of (OH, F).

***Totals have been corrected for O=F.

Table 4: Compositional data range (minima, maxima, mean and standard deviation) for dioctahedral micas ('sericite'), as alteration of spodumene, from electron microprobe analysis (CSIRO FEG hyperprobe) of samples SMCP03, 12 and 23. All values are listed as weight percent.

SMCP03,12,23 n=10				
wt%	MIN	MAX	MEAN	STD DEV
SiO2	45.93	56.50	48.66	3.76
TiO2	0.00	0.21	0.03	0.07
Al2O3	28.64	36.24	33.68	2.12
FeO	0.09	1.85	0.61	0.62
MnO	0.00	0.31	0.12	0.10
MgO	0.05	0.63	0.22	0.19
CaO	0.00	0.05	0.01	0.02
Na2O	0.06	0.40	0.21	0.12
K2O	9.25	11.48	10.65	0.60
Rb2O	0.04	1.35	0.76	0.53
Cs2O	0.02	0.05	0.04	0.02
P2O5	0.00	0.05	0.01	0.02
F	0.00	0.46	0.23	0.18
Cl	0.00	0.03	0.01	0.01
Li2O*	0.00	0.14	0.06	0.05
H2O**	4.20	4.67	4.39	0.18
Total***	98.27	101.57	99.53	1.11

*Li_2O calculation by the method of Tischendorf et al. (1997)
**H_2O calculation by the method of Tindle and Webb (1990)
***Totals have been corrected for O=F

961 Table 5: Compositional data range (minima, maxima, mean and standard deviation) for lepidolite
962 (trioctahedral mica class) from electron microprobe analysis. Data presented here are from the spatially
963 adjoining sample SMCP171 in addition to SMCP172. All values are listed as weight percent.

	SMCP171/172 n=29			
	MIN	MAX	MEAN	STD DEV
SiO2	46.46	57.12	51.60	1.80
TiO2	0.00	0.00	0.00	0.00
Al2O3	17.30	32.81	23.90	2.68
FeO	0.00	0.30	0.03	0.07
MnO	0.00	0.29	0.10	0.06
MgO	0.00	0.86	0.11	0.22
CaO	0.00	0.30	0.06	0.10
Na2O	0.07	0.27	0.14	0.04
K2O	9.11	10.77	9.47	0.31
SrO	0.00	0.12	0.04	0.04
Rb2O	1.06	4.40	3.69	0.62
Cs2O	0.02	1.15	0.77	0.21
P2O5	0.05	0.28	0.17	0.12
F	2.67	5.36	4.19	0.73
Tl2O	0.00	0.06	0.03	0.03
Li2O*	3.78	6.84	5.26	0.52
H2O*	1.97	4.57	2.55	0.52
Total**	99.17	100.99	100.07	0.52

964 *Li_2O and H_2O calculation by the method of Tindle and Webb (1990)
965 **Totals have been corrected for O=F
966
967
968
969

Figure 1

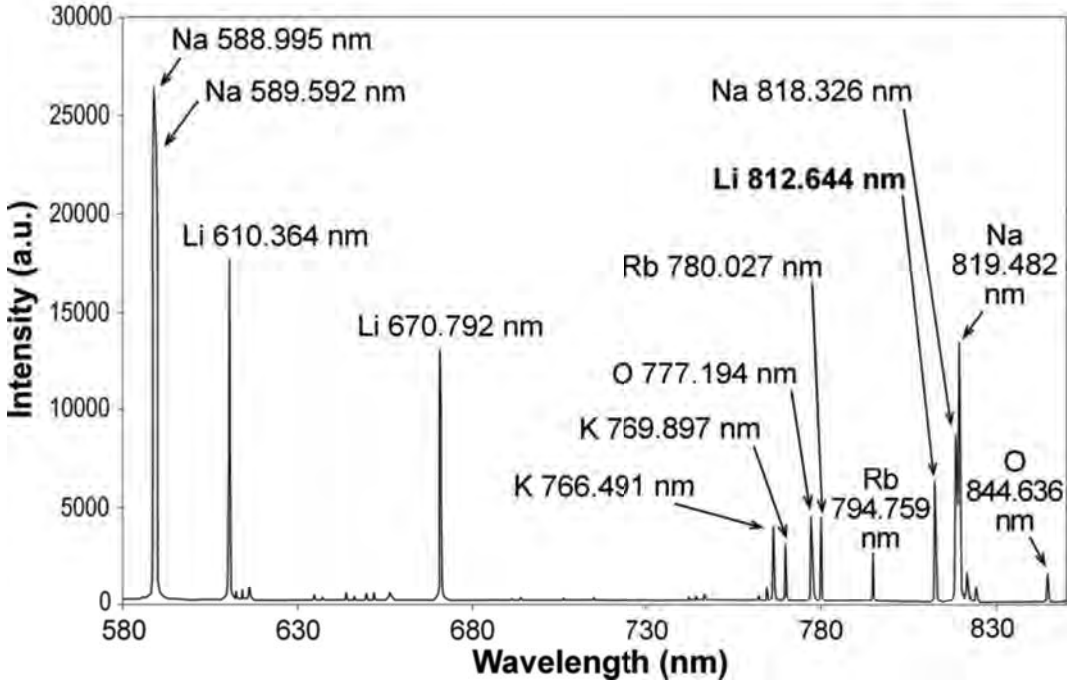
Intensity (a.u.)
30000
25000
20000
15000
10000
5000
0
580
630
680
730
780
830
Wavelength (nm)
Na 588.995 nm
Na 589.592 nm
Li 610.364 nm
Li 670.792 nm
K 766.491 nm
K 769.897 nm
O 777.194 nm
Rb 780.027 nm
Rb 794.759 nm
Na 818.326 nm
Li 812.644 nm
Na 819.482 nm
O 844.636 nm

Figure 2

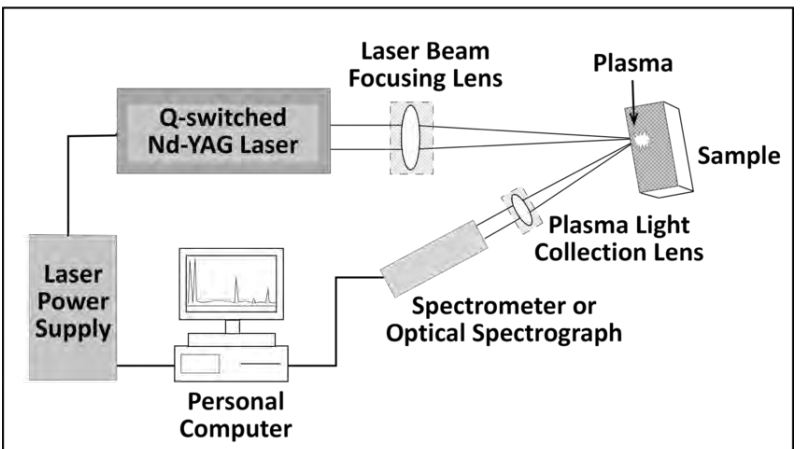
Laser Beam
Focusing Lens
Plasma
Q-switched
Nd-YAG Laser
Sample
Plasma Light
Collection Lens
Laser
Power
Supply
Spectrometer or
Optical Spectrograph
Personal
Computer

Figure 3

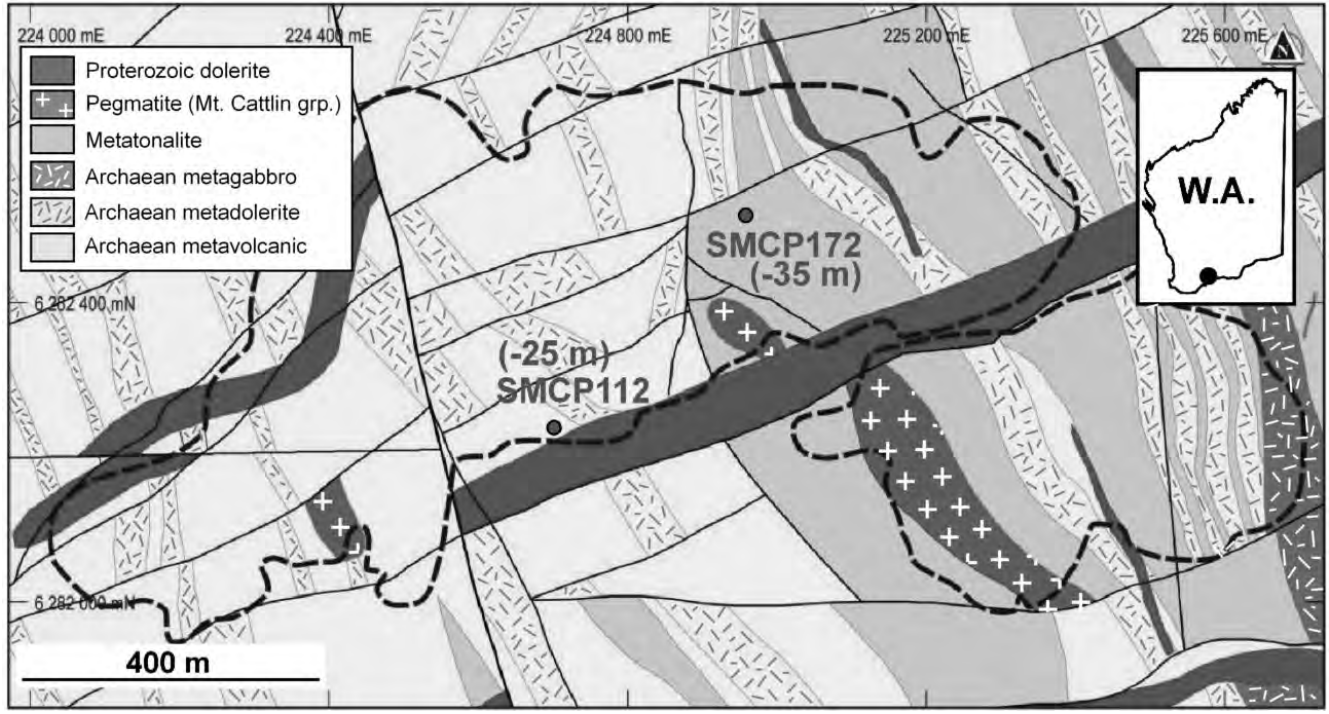
224 000 mE
224 400 mE
224 800 mE
225 200 mE
225 600 mE
Proterozoic dolerite
Pegmatite (Mt. Cattlin grp.)
Metatonalite
Archaean metagabbro
Archaean metadolerite
Archaean metavolcanic
6 282 400 mN
6 282 000 mN
SMCP172
(-35 m)
(-25 m)
SMCP112
W.A.
400 m

Figure 4(a)

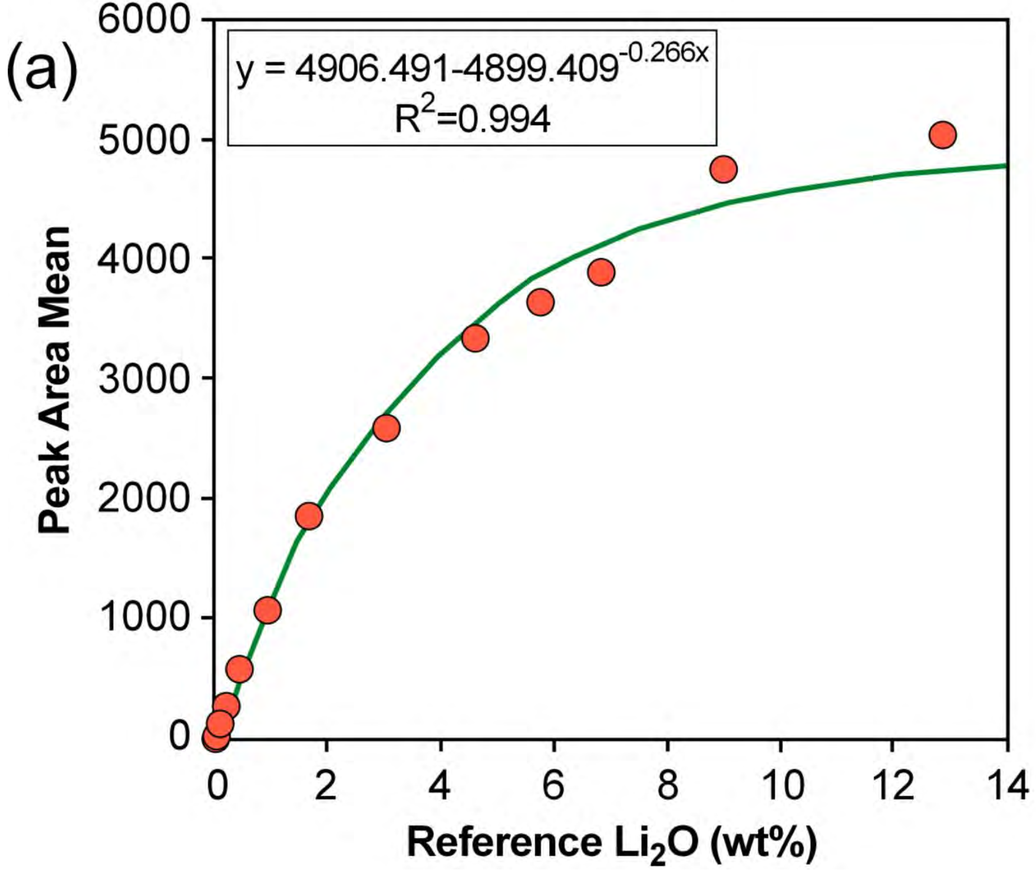

Figure 4(b)

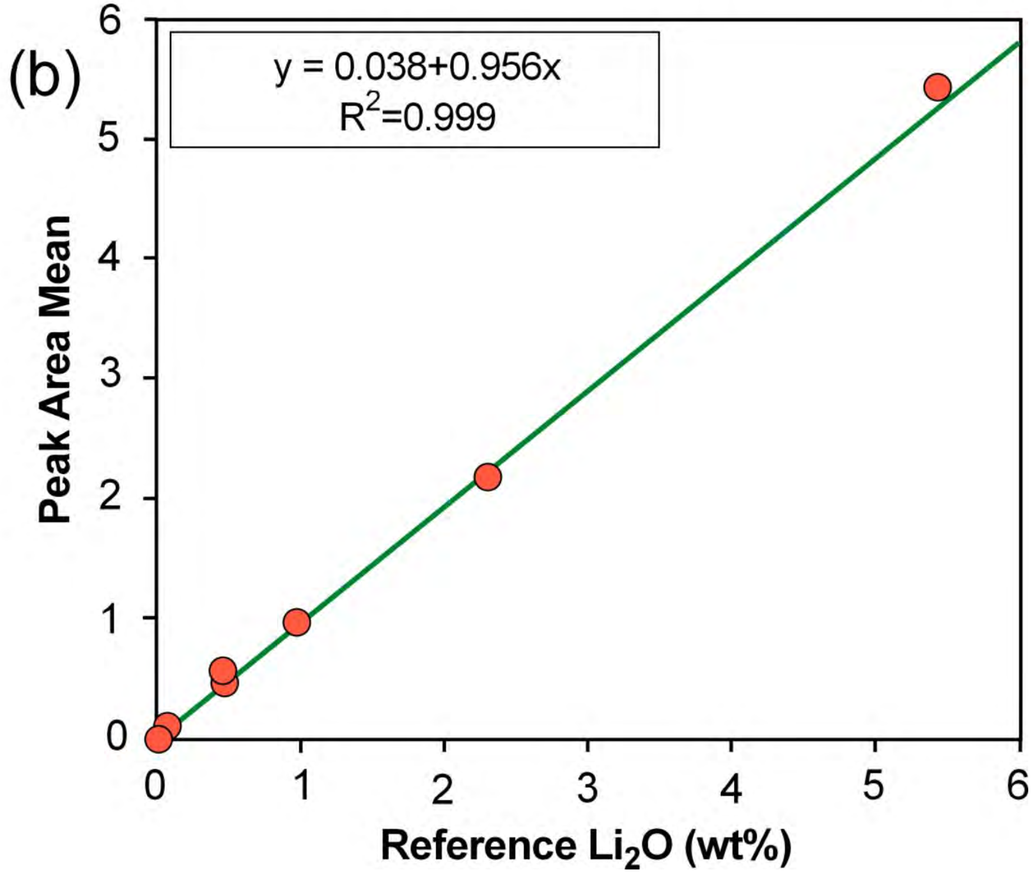

Figure 5a

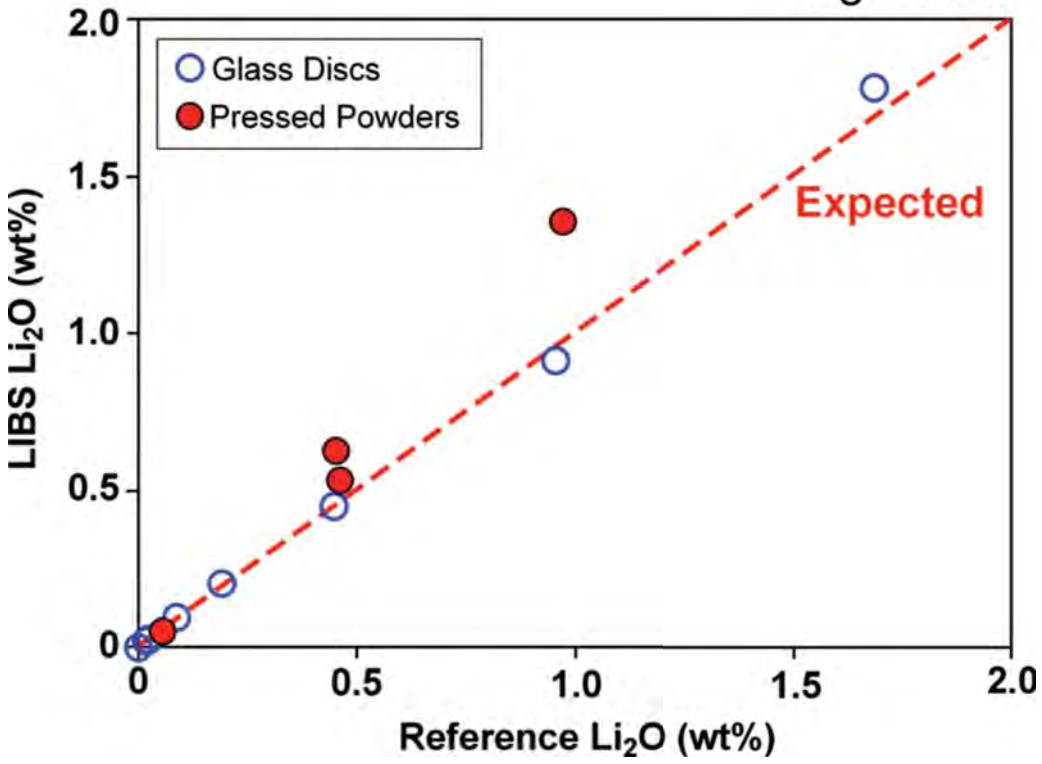
Glass Discs
Pressed Powders
Expected
LIBS Li_2O (wt%)
Reference Li_2O (wt%)
0
0.5
1.0
1.5
2.0

Figure 5b

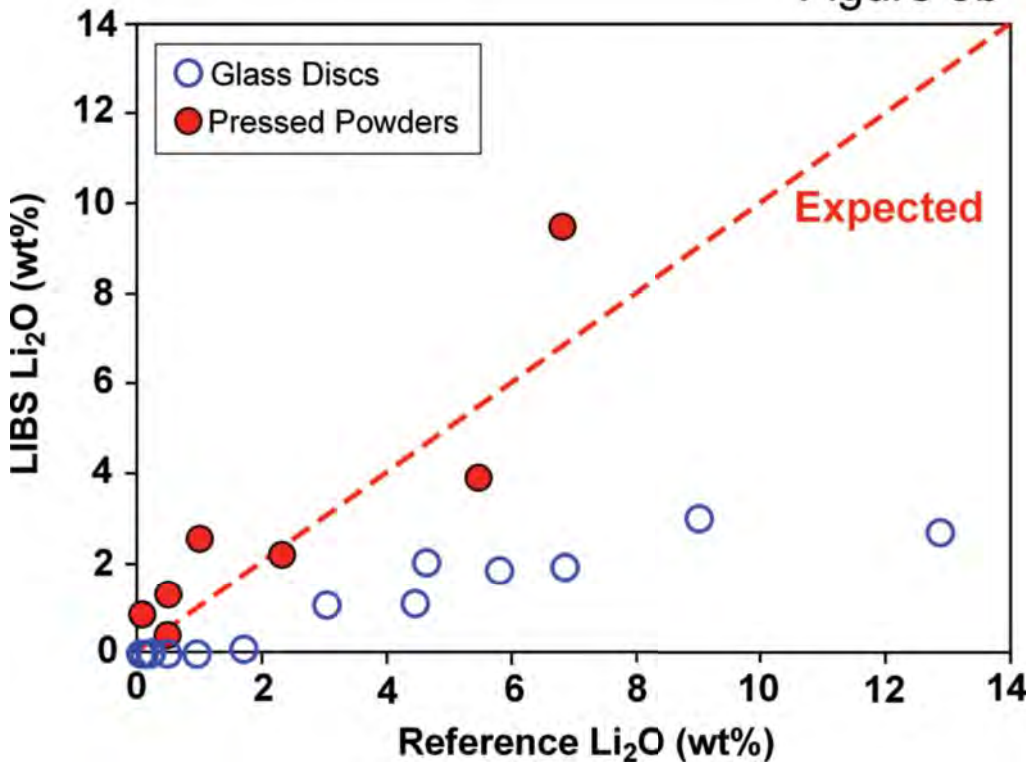
Glass Discs
Pressed Powders
Expected
LIBS Li2O (wt%)
Reference Li2O (wt%)
0
2
4
6
8
10
12
14

Figure 6

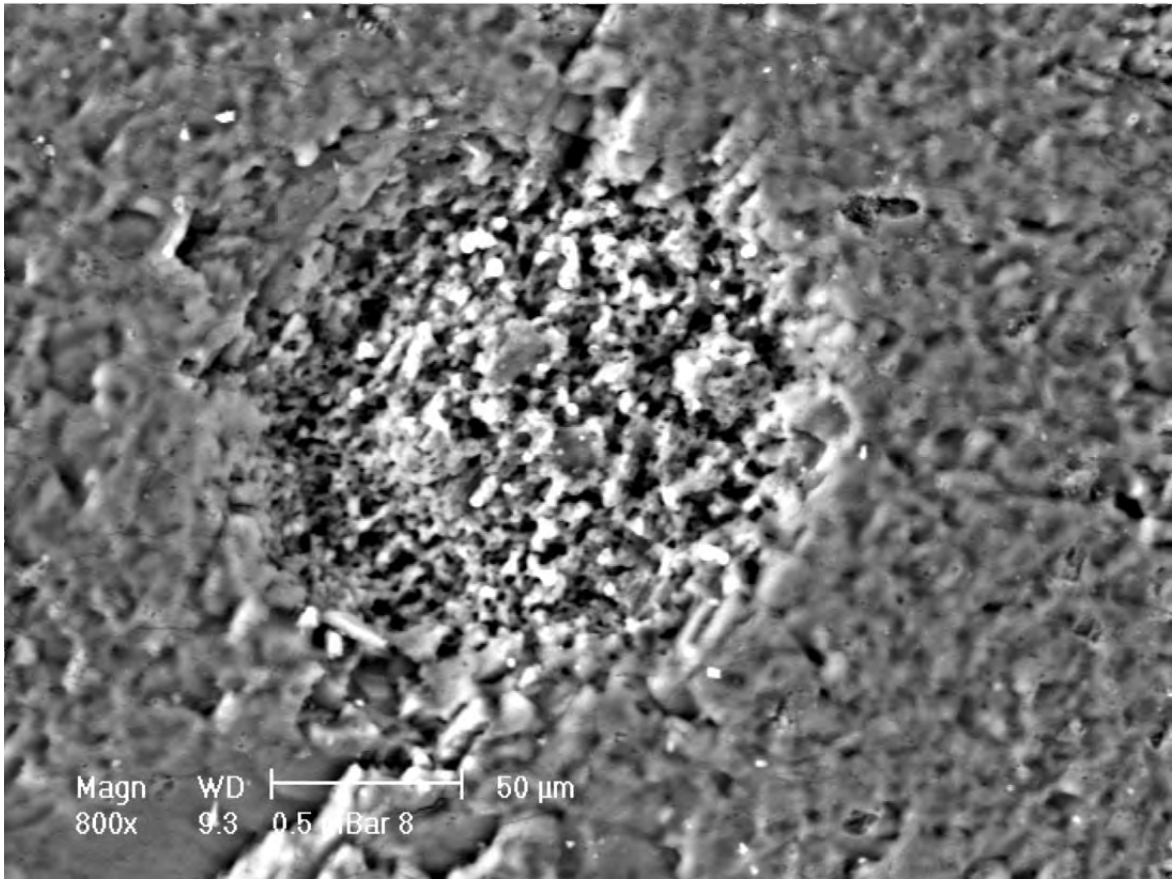

Figure 7

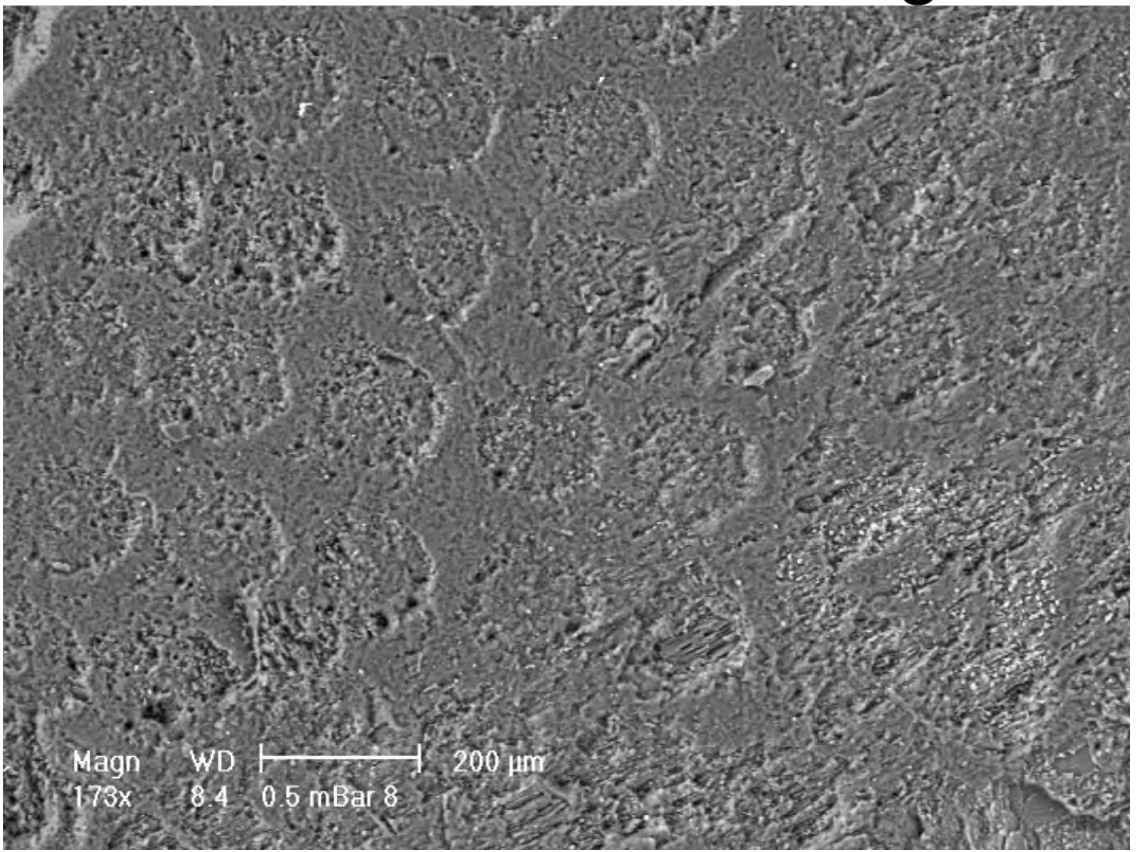

Figure 8

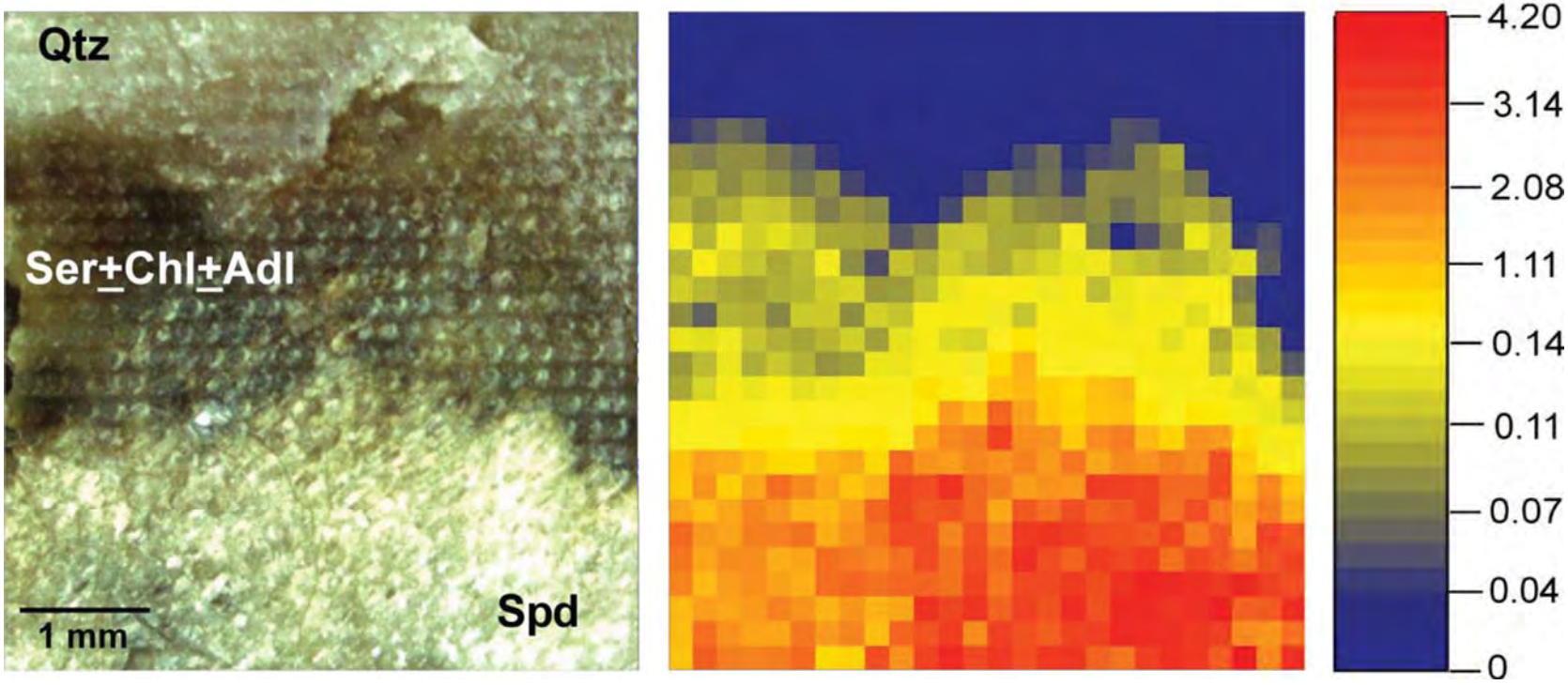

Figure 9

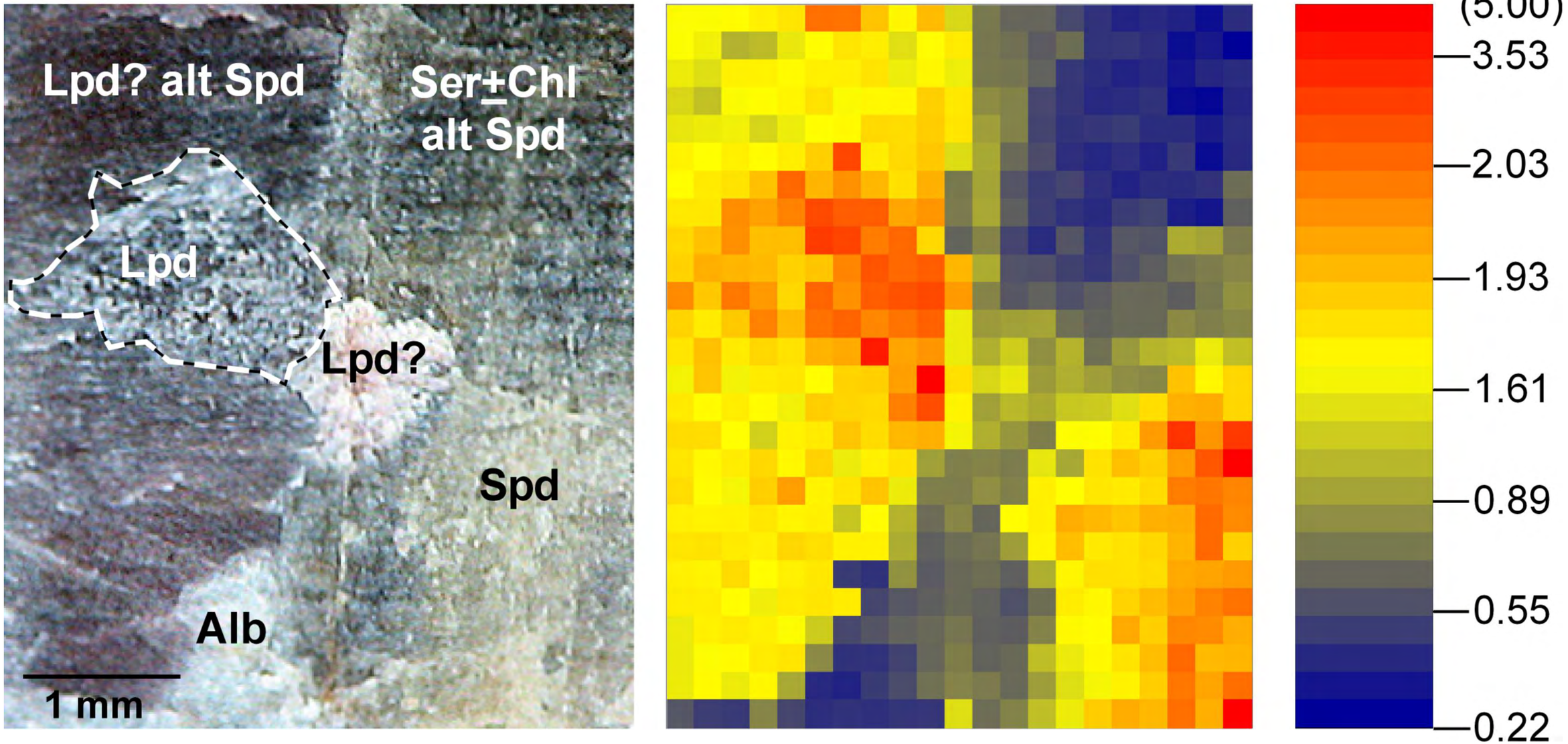
Lpd? alt Spd
Ser±Chl
alt Spd
Lpd
Lpd?
Spd
Alb
1 mm
(5.00)
3.53
2.03
1.93
1.61
0.89
0.55
0.22

Figure 10

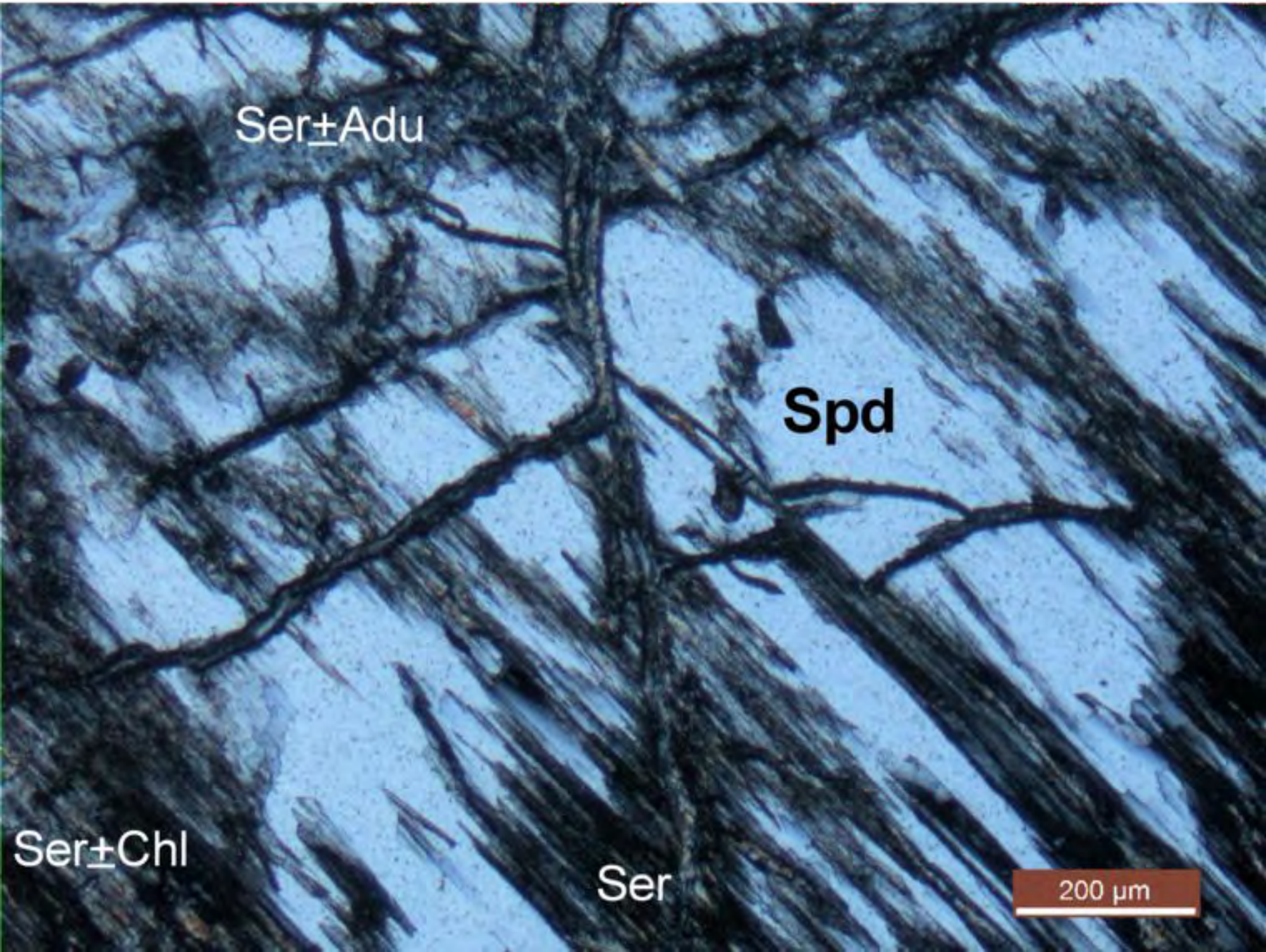

Figure 11